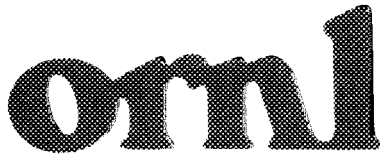




3 4456 0275017 3

ORNL/TM-10660



OAK RIDGE  
NATIONAL  
LABORATORY



# Electronic Implementation of a Closed-Loop Gas-Flow Control System

James A. Moore

OAK RIDGE NATIONAL LABORATORY  
 CENTRAL RESEARCH LIBRARY  
 CIRCULATION SECTION  
 4320N BLDG 113  
**LIBRARY LOAN COPY**  
 DO NOT TRANSFER TO ANOTHER PERSON  
 If you wish someone else to use this  
 report, send to room with report and  
 the library will arrange a loan.

Printed in the United States of America. Available from  
National Technical Information Service  
U.S. Department of Commerce  
5285 Port Royal Road, Springfield, Virginia 22161  
NTIS price codes—Printed Copy: A04 Microfiche A01

This report was prepared as an account of work sponsored by an agency of the United States Government. Neither the United States Government nor any agency thereof, nor any of their employees, makes any warranty, express or implied, or assumes any legal liability or responsibility for the accuracy, completeness, or usefulness of any information, apparatus, product, or process disclosed, or represents that its use would not infringe privately owned rights. Reference herein to any specific commercial product, process, or service by trade name, trademark, manufacturer, or otherwise, does not necessarily constitute or imply its endorsement, recommendation, or favoring by the United States Government or any agency thereof. The views and opinions of authors expressed herein do not necessarily state or reflect those of the United States Government or any agency thereof.

ORNL/TM-10660  
Dist. Category UC-37

Instrumentation and Controls Division

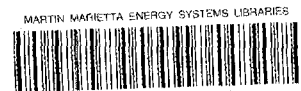
ELECTRONIC IMPLEMENTATION OF A CLOSED-LOOP  
GAS-FLOW CONTROL SYSTEM\*

James A. Moore

Date Published:  
February 1988

\*Thesis presented for the Master of Science Degree,  
University of Tennessee, Knoxville, 1985.

Prepared by the  
OAK RIDGE NATIONAL LABORATORY  
Oak Ridge, Tennessee 37831  
MARTIN MARIETTA ENERGY SYSTEMS, INC.  
for the  
U.S. DEPARTMENT OF ENERGY  
under contract No. DE-AC05-84OR21400



3 4456 0275017 3



## ACKNOWLEDGMENTS

The author expresses his gratitude to Dr. K. H. Burrell for his theoretical investigation of the gas flow measurement method; to Dr. P. H. Edmonds for his support of the project; to Dr. G. R. Dyer for his technical consultation and assistance; to D. E. Weber and W. H. Wagner for fabrication of the equipment; and to Dr. P. K. Mioduszewski, Dr. L. C. Emerson, J. L. Yarber, and J. E. Simpkins for using the system and gathering experimental data.

Gratitude is also expressed to Dr. E. J. Kennedy and Dr. J. M. Googe of the Electrical Engineering Department, University of Tennessee, for their assistance in analyzing the system and preparing this report.



## ABSTRACT

The fast gas-injection system on the ISX Tokamak at Oak Ridge National Laboratory injects controlled amounts of impurity gases into a hydrogen plasma to study particle transport physics within the plasma. Since for a given discharge the plasma lasts only a fraction of a second at near vacuum pressures, fast, accurate control of the impurity injection rate is essential for discharge stability and meaningful quantitative analysis.

The gas-injection control system in place on this experiment exhibited excessive drift, poor maintainability, and limited versatility. This report investigates the design of an improved electronic control system featuring higher loop gain, automatic drift cancellation, high reliability and maintainability, fault protection, and increased versatility through computer control. The circuitry designed for this system exhibits negligible electronic noise and drift while providing repeatable response on a millisecond time scale. Unconditional stability and graceful recovery from saturation have been observed. Problems with noise intrusion and thermal sensitivity remain. Further development will be required before an operational system can be fabricated.



## CONTENTS

1.	INTRODUCTION . . . . .	1
2.	PRINCIPLE OF OPERATION . . . . .	2
3.	SYSTEM DESIGN . . . . .	5
3.1	Gas Valve . . . . .	6
3.2	Pressure Transducer . . . . .	6
3.3	Auto-Zero Preamplifier . . . . .	10
3.4	Error Amplifier . . . . .	11
3.5	Differential Line Receiver . . . . .	14
3.6	High-Voltage Operational Amplifier . . . . .	15
3.7	Valve Drive Gate . . . . .	17
3.8	System Overview . . . . .	17
4.	ANALYSIS OF SYSTEM COMPONENTS AND RESPONSE . . . . .	18
5.	PRELIMINARY TEST RESULTS . . . . .	42
6.	CONCLUSIONS . . . . .	46
	REFERENCES . . . . .	47



## FIGURES

1.	Simplified system block diagram . . . . .	5
2.	Gas valve characteristics . . . . .	7
3.	Gas injector drawing . . . . .	8
4.	Transducer data sheet . . . . .	9
5.	Preamplifier basic schematic diagram . . . . .	10
6.	Preamplifier full schematic diagram . . . . .	12
7.	Error amplifier schematic diagram . . . . .	13
8.	Line receiver schematic diagram . . . . .	14
9.	High voltage operational amplifier schematic diagram . . . . .	16
10.	Valve drive gate schematic diagram . . . . .	17
11.	General configuration of a series feedback amplifier . . . . .	18
12.	Feedback diagram for Miller's Theorem . . . . .	21
13.	General configuration of a shunt feedback amplifier . . . . .	23
14.	Passive gain CKT of shunt feedback amplifier . . . . .	23
15.	Detailed system block diagram . . . . .	29
16.	CSMP III simulation of gas injector open-loop pulse response . . . . .	31
17.	CSMP III simulation of closed-loop system rise time . . . . .	32
18.	CSMP III simulation of closed-loop system response to a 150-ms demand pulse . . . . .	36
19.	CSMP III simulation of closed-loop system response to a 200-ms unipolar sawtooth demand signal . . . . .	39
20.	Laboratory prototype response waveforms for short-duration demand signals . . . . .	43
21.	Laboratory prototype response waveforms for long-duration demand signals . . . . .	44
22.	Thermal and noise intrusion waveforms for the system installed on ISX-B . . . . .	45



## 1. INTRODUCTION

The original purpose of this gas flow control system was to inject a highly collimated jet of hydrogen gas into a Tokamak plasma. It was expected that this controlled hydrogen injection would enhance the plasma density and reverse the transport of impurity ions toward the center of the plasma.<sup>1,2</sup> Since the original application, this system has been applied to numerous different gases and experiments. Indeed, measurement and control of minute amounts of gas on a millisecond time scale are interesting and challenging problems in their own rights.

Many modifications were added to the ISX Tokamak's original gas injection system between 1977 and 1983 in an effort to enhance its accuracy and usability. Finally, all of the cures became worse than the original disease. This was evident because a zero drift problem remained, the flow measurements obtained did not correlate well with the pressure rise observed in the vacuum vessel during calibration attempts, and the many modifications were sparsely documented. Confidence in the system diminished to the point that a complete redesign of the system electronics was ordered in May 1983.

This report investigates the design of an electronic instrumentation and control system to upgrade the usability of the fast gas-injection system on ISX-B. The project had three specific goals:

1. To provide a system whose response is limited by the gas valve response and injector plumbing alone;
2. To provide control and instrumentation electronics that require no periodic operator attention; and
3. To provide inputs, outputs, and safeguards that would permit easy interface with computer controlled flow demand and data acquisition hardware.

Design constraints were that the gas valve, pressure transducer, and associated plumbing would continue to be used.

Section 2 briefly reviews the physics governing the gas flow in this apparatus and the equations that are used to model it.

Section 3 describes the system components. Emphasis is placed on those circuits designed specifically for this project, while brief information on previously existing circuits and equipment is included for completeness.

Section 4 is a computer aided analysis of the complete system response.

Section 5 presents the experimental results.

Section 6 summarizes project results and presents conclusions and recommendations for future development efforts.

## 2. PRINCIPLE OF OPERATION

There were three major considerations in the mechanical design of the gas injector: the rise time of the flow, the physical size of the apparatus, and the measurability of the flow. In his analysis Burrell<sup>1</sup> investigated two basic approaches: molecular flow using large-diameter piping at low pressure and laminar flow using small-diameter piping at high pressure. The latter was chosen because of its important size advantage and because the pressure measurement (from which the flow would be inferred) is much easier to make when the range spans several hundred torr. With this method, temperamental and magnetically sensitive ion gages are avoided in favor of a small strain-gage pressure transducer.<sup>1</sup>

Since gases have some viscosity, a very narrow pipe (0.7-mm-diam in this case) can result in a viscous, incompressible flow which can be modeled by the same equations used to model laminar fluid flow in a pipe.<sup>3</sup>

J. L. M. Poiseuille and Gotthilf Hagen independently derived the volume flow rate equation for laminar fluid flow in the early 1800s.<sup>4</sup> Now known as the Poiseuille equation, it relates the volume flow rate to the differential pressure and pipe length. It is given by

$$Q' = \frac{\pi a^4 dp}{8\eta dl} ,$$

where  $Q'$  is the volume rate,  $a$  is the pipe radius,  $\eta$  is the fluid viscosity,  $p$  is the pressure, and  $l$  is the pipe length.

Incompressibility is assumed in this equation.<sup>3</sup> In order for the equation to have meaning for gases, a volume-pressure flow rate is needed. Letting  $Q = Q' p$ , multiplying both sides of the equation by  $p$  and separating variables yields

$$Q dl = \frac{\pi a^4 p dp}{8\eta} .$$

Integrating over the length of the tube and over the pressure difference from end to end gives

$$\int_0^L Q dl = \int_0^P \frac{\pi a^4 p dp}{8\eta}$$

and

$$QL = \frac{\pi a^4 P^2}{16\eta} .$$

Rearranging and letting  $C = \pi a^4 / 16\eta L$  gives

$$Q = CP^2 \quad (1)$$

Invoking the continuity principle, a simple model for the time response of the pressure in the presence of an imposed flow into one end of the pipe is

$$\frac{d}{dt} PV = -CP^2 + Q(t) \quad , \quad (2)$$

where  $V$  is the sum of any trapped volume plus one-half the volume of the pipe (the one-half is due to the linear fall in pressure across the pipe, a property of Poiseuille flow<sup>1</sup>).

The left-hand term in the equation models the density in the pipe, while  $Q(t)$  is the flow entering the pipe and  $-CP^2$  is the flow leaving the pipe. By setting  $Q(t) = 0$  and establishing  $P_0$  as the initial condition, the fall time of the pressure after the valve closes can be obtained. With  $Q(t) = 0$ , separating variables yields

$$\frac{VdP}{P^2} = -Cdt \quad ,$$

and indefinite integration yields

$$\frac{-V}{P} + C_1 = -Ct + C_2 \quad .$$

Solving this equation for  $P$  and combining constants gives

$$P(t) = \frac{V}{Ct + C_3} \quad .$$

Imposing the initial condition of  $P(0) = P_0$  and choosing  $C_3$  such that  $V/C_3 = P_0$ , we obtain

$$P(t) = \frac{P_0}{1 + \frac{P_0 C}{V} t} \quad . \quad (3)$$

In this form, one easily sees that the pressure is well behaved and varies as  $1/t$  after the valve closes; consequently, the flow drops as  $1/t^2$ . Substituting the appropriate constants for  $C$  indicates that satisfactory response time should be obtained with the geometry chosen in this design.

The solution to Eq. 2 under an imposed flow [ $Q(t) > 0$ ] is cumbersome and yields little insight. It does, however, reveal that the response

is logarithmic. Intuitively, the forced response should be no slower than the natural response, provided a sufficient flow can be imposed.

Provided laminar flow dominates, the fundamental equations indicate that the flow can be initiated and terminated rapidly. Further, they imply that the flow can be regulated by controlling the pressure downstream of a fast, modulatable valve.

## 3. SYSTEM DESIGN

The simplified block diagram of the flow control system is depicted in Fig. 1. The configuration is a standard linear feedback control system. An unusual feature of this design is that the gas itself is part of the signal path, and hence system response and stability are dependent upon a good mechanical design of the gas injector. The interesting circuit in this system from an electronics point of view is the transducer preamplifier, which is designed to be mounted remotely at the pressure transducer. It provides excitation for the transducer and incorporates a local feedback loop which automatically zeros the transducer's strain-gage bridge and eliminates drift. While the system's basic concept is straightforward, the actual implementation is slightly more complex because of valve and transducer limitations. Each of the major components is discussed in this section. The block diagram of the final system configuration is included in Sect. 4, which is an analysis of the system response.

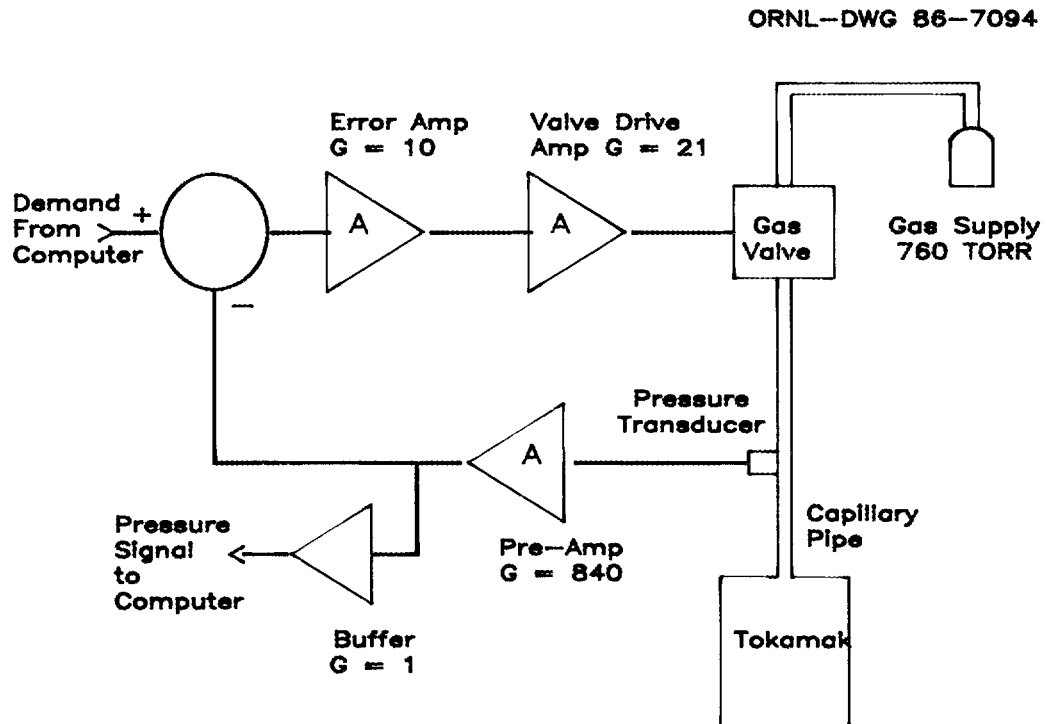


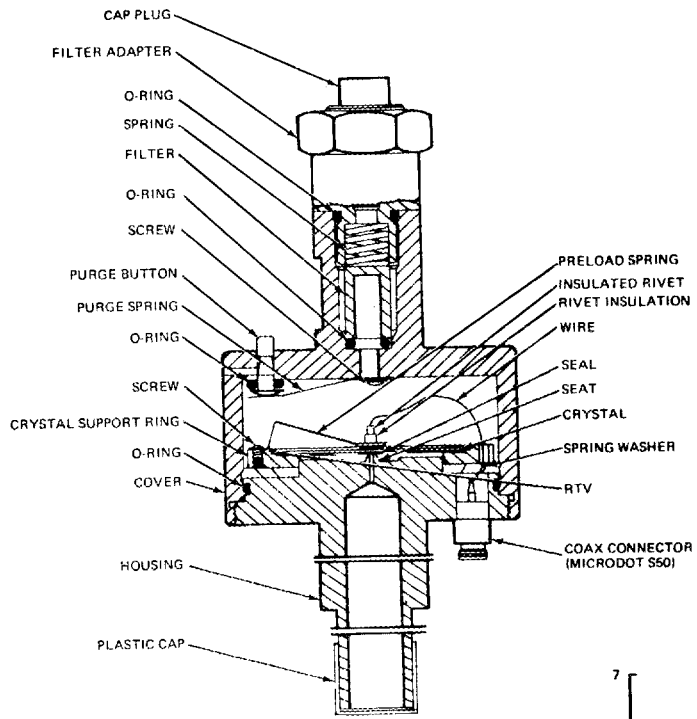
Fig. 1. Simplified system block diagram.

### 3.1 Gas Valve

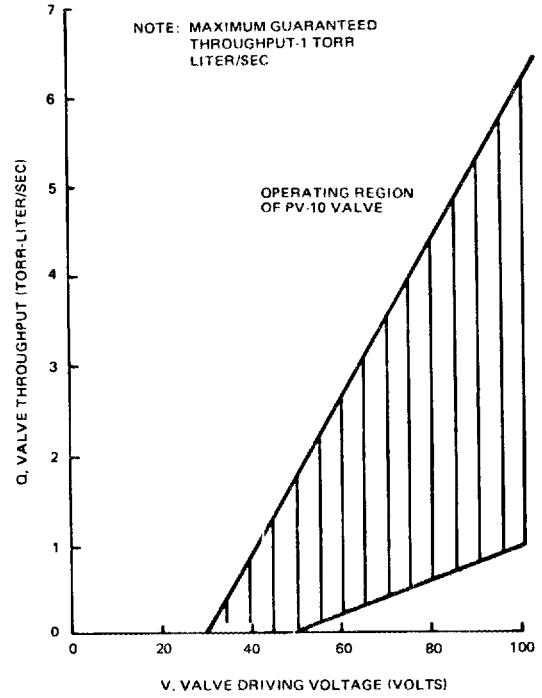
The modulatable gas valve chosen for ISX is Veeco Instruments Model PV-10. Its fast response and modulatable aperture make the system possible. The manufacturer claims the valve is capable of making the transition from closed to fully open in 2 ms, and that the throughput of the valve is essentially a linear function of the control voltage over a range of 30 to 100 V (see Fig. 2). This is accomplished by using the control voltage to warp a piezoelectric crystal over a soft rubber seat. The crystal is spring loaded and the crystal warpage is against the inlet pressure. It has been experimentally observed that the valve does, in fact, have essentially the advertised response characteristics. Unfortunately, it also has a number of unadvertised characteristics as well. Among these are a tendency to stick closed after a few hours of sitting in the closed position. When this occurs, more than 100 V may be required to open the valve within the desired time interval. The valve, as implied by the graph in Fig. 2, also exhibits considerable hysteresis so that repeating the drive signal does not imply repetition of the throughput. As has been mentioned, the valve opens against the flow. It is apparent that the head pressure feeding the valve contributes significantly to the force closing the valve (see Fig. 2). Thus at low head pressure (<500 torr) the valve can fail to seal when drive voltage is removed. This necessitates the application of a negative bias to force the valve to close. These three limitations complicate the system electronics somewhat by necessitating closed-loop operation, a bipolar valve drive amplifier with a +150-V output capability, and a flow-sensing pulse or "popping" circuit to force a stuck valve open. Finally, a negative output offset must be provided to ensure that the valve closes reliably. The schematic diagram of the resulting error amplifier is included later in the section on the error amplifier.

### 3.2 Pressure Transducer

The pressure transducer used on the ISX gas injector is an Entran Devices Model EPS-1032 consisting of a miniature strain-gage bridge circuit mounted in the tip of a hollow size 10-32 machine screw. Its full-scale range is 0 to 15 psia, and its sensitivity is nominally 2 mV/psia. This transducer is an impressive device with a resonant frequency well beyond anything needed in this application. However, its major flaw is temperature sensitivity. The thermal drift specification for this device assumes that the compensation network in the output lead thermally tracks the tip temperature. In this application that assumption is totally invalid. Referring to the gas injector drawing (Fig. 3), the gas flow impinges directly on the transducer tip, which rapidly cools it independent of the compensation module. The severe ramifications of this cooling are discussed in Sect. 5. The manufacturer's data sheet for the transducer (Fig. 4) is included for information.



PV-10 VALVE CROSS SECTIONAL DIAGRAM



PV-10 VALVE THROUGHPUT VS VALVE DRIVING VOLTAGE CURVE

Fig. 2. Gas valve characteristics.

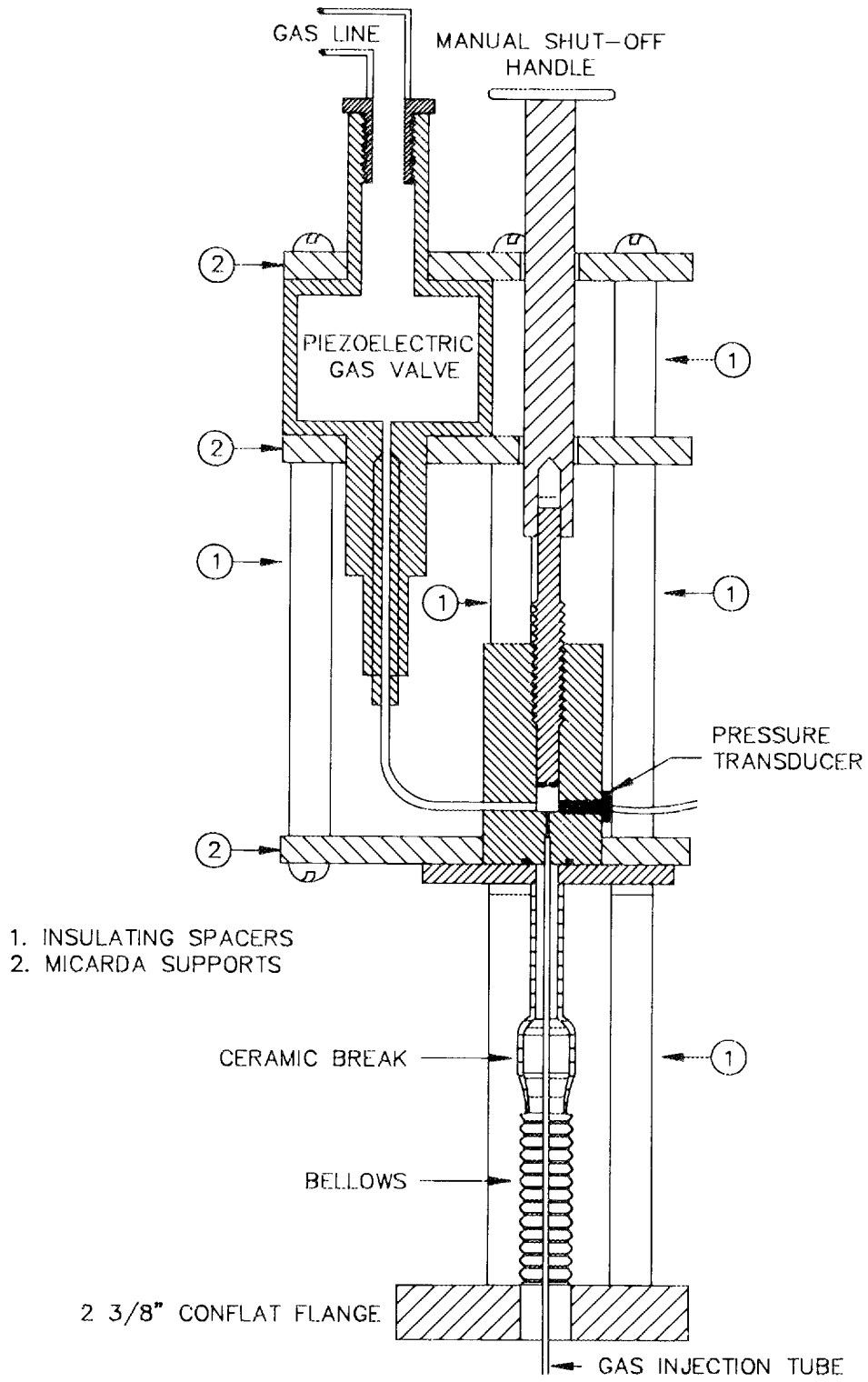
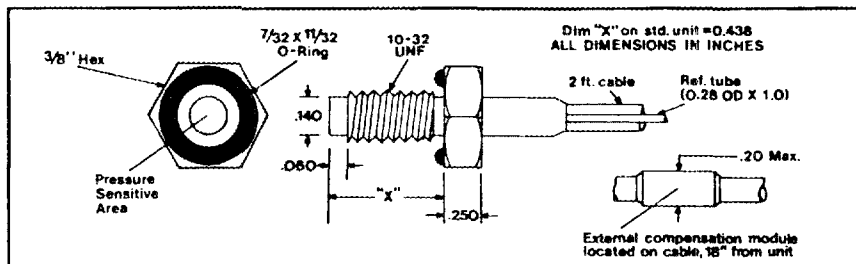


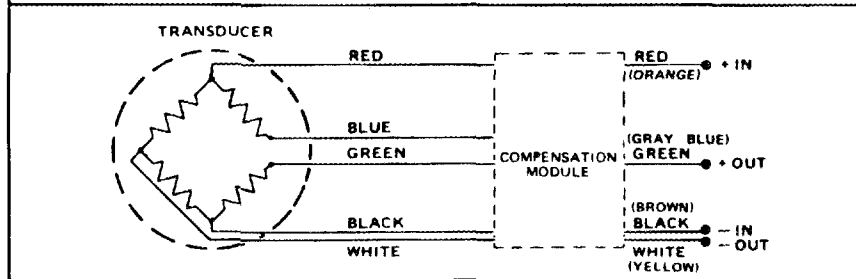
Fig. 3. Gas injector drawing.

**SPECIFICATIONS**

MODEL	EPS-1032 -5	EPS-1032 -10	EPS-1032 -15	EPS-1032 -30	EPS-1032 -50	
<b>RANGE</b>	psi	5	10	15	30	50
<b>OVER-RANGE</b>	psi	50	50	50	60	100
<b>SENSITIVITY</b>	mV FS. (nom.)	15	25	30	60	100
<b>RESONANT FREQUENCY (nom.)</b>		45 KHz	50 KHz	65 KHz	70 KHz	75 KHz
<b>INPUT IMPEDANCE (nom.)</b>		500 ohms: 280 ohms optional				
<b>OUTPUT IMPEDANCE (nom.)</b>		250 ohms: 140 ohms optional				
<b>EXCITATION</b>		6.0 V DC or AC: For other excitation voltages, specify at time of order.				
<b>COMBINED NON-LINEARITY and HYSTERESIS</b>		±1% F.S.				
<b>REPEATABILITY</b>		0.25%				
<b>RESOLUTION</b>		Infinite				
<b>THERMAL ZERO SHIFT</b>		±4% F.S./100°F	±3% FS/100°F	±2% F.S./100°F		
<b>THERMAL SENSITIVITY SHIFT</b>		±2%/100°F				
<b>COMPENSATED TEMP. RANGE</b>		80°F to 180°F (25°C to 80°C)			Can be compensated over any portion of operating temp.	
<b>OPERATING TEMP. RANGE</b>		-40°F to 250°F (-40°C to 121°C)			Higher and lower temperature ranges are available.	



**EPS-1032 I-XX-(XX)**  
 Series      Internal Compensation Option      Range      Custom Screw Length Option desired length (Dimension "X") in inches (from .25 to 1.50).



**Entran Devices, Inc.**      145 Paterson Ave. Little Falls, N. J. 07424 (201) 785-4060      Specifications subject to change without notice.

Fig. 4. Transducer data sheet.

### 3.3 Auto-Zero Preamplifier

Because of the low signal level of the transducer, it was desirable to locate a high-gain preamplifier as near as possible to the transducer ( $A_1$  in Fig. 1). One of the significant problems with the original design was the need to rebalance the transducer bridge circuit as often as possible. This balance must be highly accurate because of the high gain required. One of the system requirements was automatic zeroing. High differential mode gain, high common mode rejection, and low noise were also important characteristics.

Excitation for the transducer bridge was also incorporated into the preamplifier circuit.

The design was begun with the choosing of a circuit configuration for the differential preamplifier. The circuit in Fig. 5 was chosen primarily for its high common mode rejection and high input impedance. Precision Monolithics Model OP-07 was chosen for the first stage amplifiers to ensure low noise and high accuracy while allowing the circuit to be constructed from readily available parts. Analysis by superposition yields a midband gain of

$$g = \frac{R_4 + 2R_3}{R_4} \frac{R_1}{R_2}$$

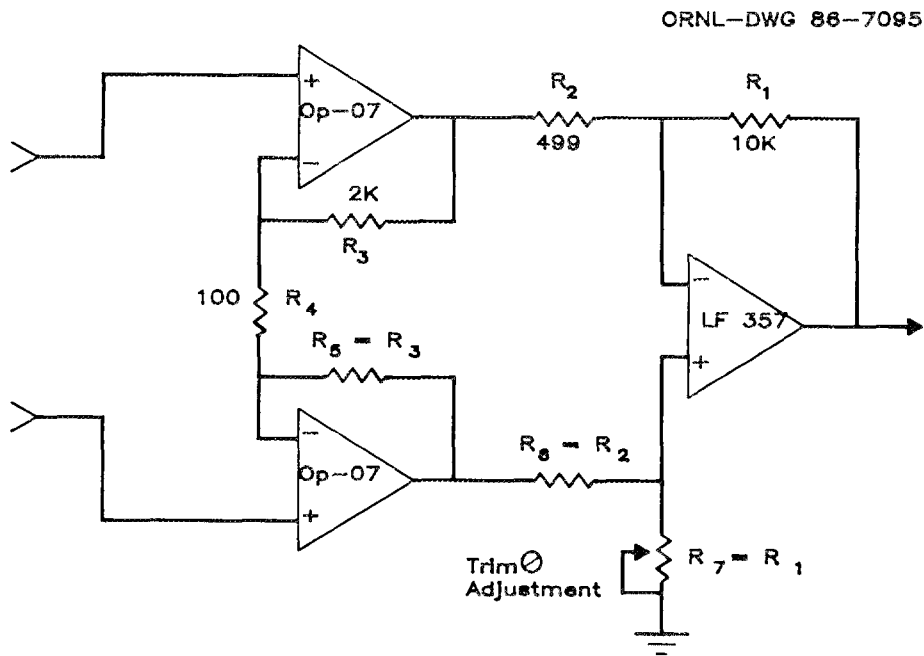


Fig. 5. Preamplifier basic schematic diagram.

This approximation is satisfactory for frequencies below 10 kHz, which is about ten times the anticipated signal bandwidth.

Theoretically, the common mode gain of the circuit can be zero. In practice the dc common mode gain can be nulled to an immeasurable level using the single trim pot,  $R_7$ . Common mode rejection at 10 kHz exceeds 60 dB. This configuration has the disadvantage of limited common mode input voltage range ( $\pm V_{CC}$ ), but this was not a significant disadvantage for this application, considering the low source impedance and very short cable connected between the pressure transducer and the preamplifier.

The unique feature of this preamplifier, and the one which forced the design of a special preamplifier for this application, is the automated bridge-balancing circuit (see Fig. 6). Requirements for this circuit were that the strain-gage bridge be balanced and maintain balance without operator action and that the balancing scheme not affect the precision of the pressure measurement or degrade the signal-to-noise ratio.

The balancing circuit of Fig. 6 accomplishes all of these objectives. It consists of two precision current sources and an integrator in an overall feedback loop. One current source, consisting of  $U_3$ ,  $J_1$ , and  $R_{12-14}$ , is fixed at 517  $\mu\text{A}$  and is used to guarantee that the initial imbalance will be in favor of a particular side of the bridge. The integrator,  $U_1$ , then samples the output voltage and integrates it with a 10-s time constant ( $R_8 C_1 \approx 10 \text{ s}$ ). The output of  $U_1$  drives the second current source consisting of  $U_2$ ,  $J_2$ , and  $R_{11}$ . This current source ranges from approximately 130  $\mu\text{A}$  to nearly 2 mA as required to stabilize the output of  $U_6$  to 0 V. By using an LF 356 for the integrator and trimming its input offset with  $R_{10}$ , the output offset voltage from  $U_6$  does not exceed  $\pm 20 \text{ mV}$ . This is equivalent to ac coupling with a low-frequency roll-off value of 17 mHz. The slew rate of the balancing circuit is limited by the two germanium clamping diodes,  $D_1$  and  $D_2$ , which greatly reduce the integrator's response to a real pressure signal during a pulse. Because of the extremely high impedance of the current sources ( $U_3$ - $J_1$  and  $U_2$ - $J_2$ ) and the low impedance of the strain-gage bridge, the noise performance of the preamplifier is not compromised by the auto-zero circuit.

### 3.4 Error Amplifier

The error amplifier for this system ( $A_2$  of Fig. 1) was also custom designed. Its schematic diagram is depicted in Fig. 7. It incorporates a unity gain differential input amplifier,  $U_4$ , to follow the flow demand signal; a dedicated buffer-follower,  $U_3$ , to feed the data system; and a popping circuit to ensure rapid opening of a stuck valve. A negative output offset voltage is provided by  $R_9$  in conjunction with  $U_2$  to guarantee that the gas valve closes when the demand signal reaches zero and to prevent small inadvertent spurts of



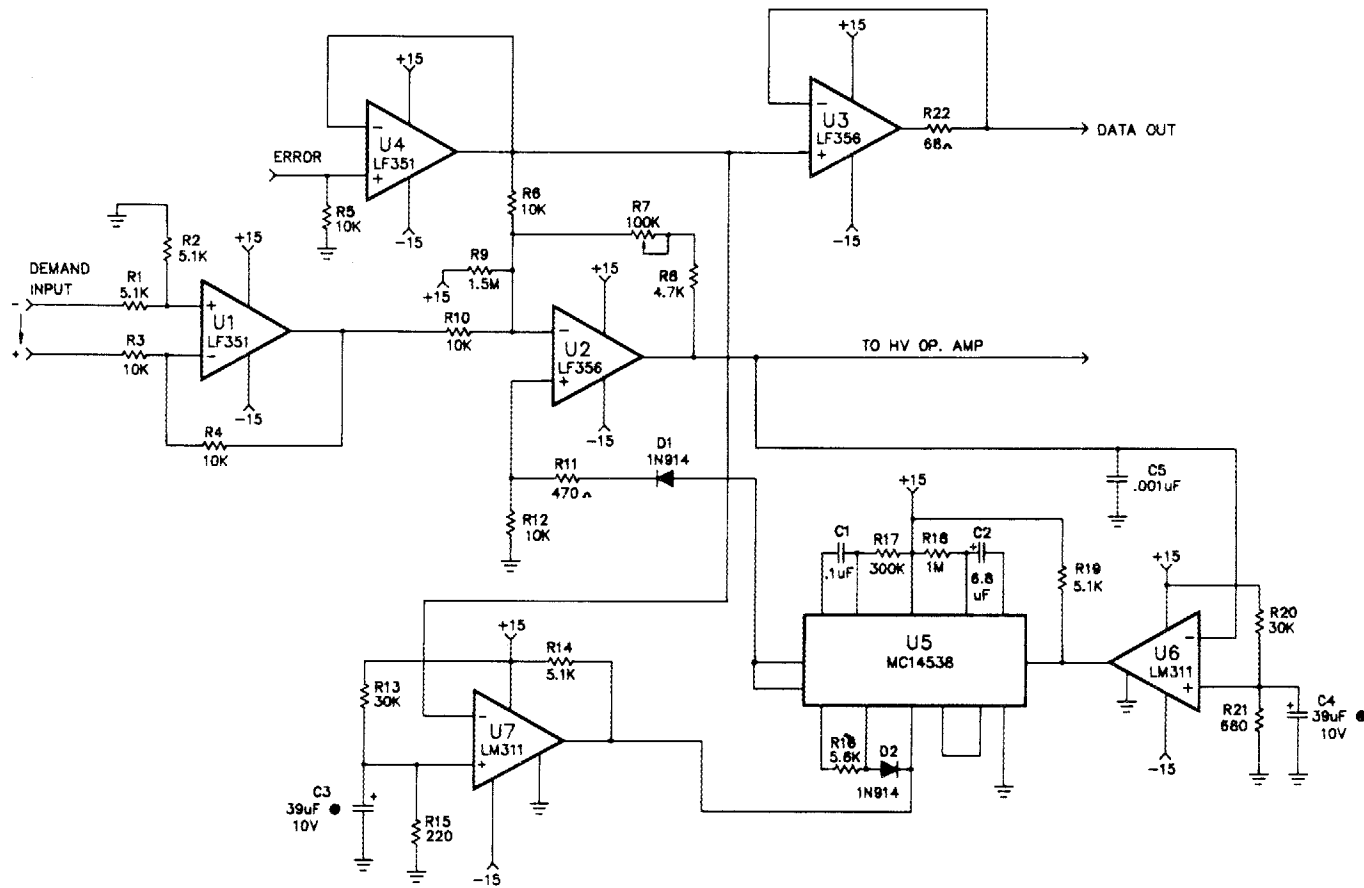


Fig. 7. Error amplifier schematic diagram.

gas due to noise intrusions into the system. The error amplifier,  $U_2$ , operates at a maximum gain slightly greater than 10. A unique feature of the error amplifier board is the valve popping circuit consisting of a dual nonretriggerable monostable multivibrator,  $U_5$ , and two comparators,  $U_6$  and  $U_7$ . One comparator ( $U_6$ ) samples the output of the error amplifier and switches when the level indicates gas flow is desired. The output of  $U_6$  drives the falling edge trigger of the CMOS monostable multivibrator,  $U_5$ , which has an output pulse width of 30 ms ( $C_1R_{17}$ ). The second comparator,  $U_7$ , samples the pressure signal and switches when flow is established. This comparator resets the first monostable multivibrator and simultaneously triggers another monostable multivibrator, which continues to hold the first monostable multivibrator in reset for about 6 s ( $C_2R_{18}$ ). This prevents popping the valve again in case a complex demand waveform momentarily drives the valve control signal to zero during a particular shot.

### 3.5 Differential Line Receiver

A differential amplifier is used between the preamplifier and the error amplifier (between  $A_1$  and  $A_2$  in Fig. 1) in order to ensure that only signal currents flow in the signal leads connecting the two amplifiers. Features of the circuit include high common mode voltage range, unity gain, and balance adjustments for both ac and dc common mode rejection. This circuit is a standard circuit developed by G. R. Dyer of the ORNL Fusion Energy Division and used in numerous systems for several years. It is depicted schematically in Fig. 8.

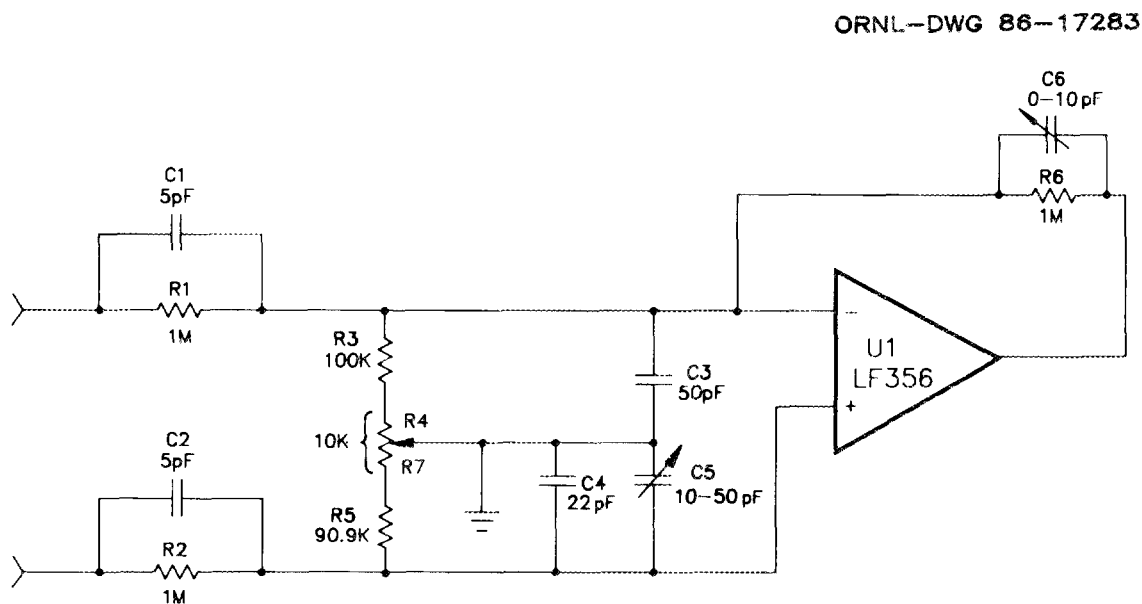


Fig. 8. Line receiver schematic diagram.

From Fig. 8, the resistive and capacitive network surrounding  $U_1$  forms a symmetric bridge circuit in which the attenuation ratios are frequency independent. For this condition to hold,  $C_6$  is adjusted so that  $R_1 C_1 = R_6 C_6$ ,  $C_5$  is adjusted so that

$$\frac{C_1}{C_3 + C_6} = \frac{C_2}{C_4 + C_5} ,$$

and  $R_4$  is adjusted so that

$$\frac{(R_4 + R_3) // R_6}{R_1 + (R_4 + R_3) // R_6} = \frac{R_5 + R_7}{R_2 + R_5 + R_7} .$$

With these conditions satisfied, both inputs to  $U_1$  are driven with the same voltage (for a common mode signal), and the common mode gain is nulled while the common mode voltage range is extended by a factor of roughly 10. For a differential mode signal, the gain is

$$\begin{aligned} \frac{R_6 // C_6}{R_1 // C_1} &= \frac{(R_5 + R_7) // (C_4 + C_5)}{(R_2 // C_2) + (R_5 + R_7) // (C_4 + C_5)} \\ &\times \frac{(R_6 // C_6) + (R_1 // C_1) // [(R_3 + R_4) // C_3]}{(R_1 // C_1) // [(R_3 + R_4) // C_3]} = 1 . \end{aligned}$$

As implied by the equations, the adjustments are interactive, and several iterative adjustments are necessary for proper operation.

### 3.6 High-Voltage Operational Amplifier

The piezoelectric valve requires a driving voltage in excess of 120 V to ensure rapid operation; hence, a driver amplifier ( $A_3$  of Fig. 1) with high-voltage output capability was required. The current required from this amplifier is very small and consists primarily of charging current for cable capacitance. A previously existing design was modified for this application. A CA3100 operational amplifier is used in the input circuit of this amplifier because of its excellent slew rate.  $U_1$  (Fig. 9) drives a high-voltage amplifier which comprises  $Q_1$  through  $Q_4$  and associated biasing circuitry. The high-frequency gain of this amplifier is rolled off by  $C_3$  feeding back to the emitters of  $Q_1$  and  $Q_2$  to preserve overall circuit stability. Diodes  $D_2$  to  $D_5$ ,  $D_7$ , and  $D_8$  provide overload protection, while  $D_6$  and  $D_10$  provide inductive load protection for  $Q_3$  and  $Q_4$ . The overall circuit gain controlled by  $R_2$ ,  $R_3$ , and  $C_1$  is analyzed in Section IV.

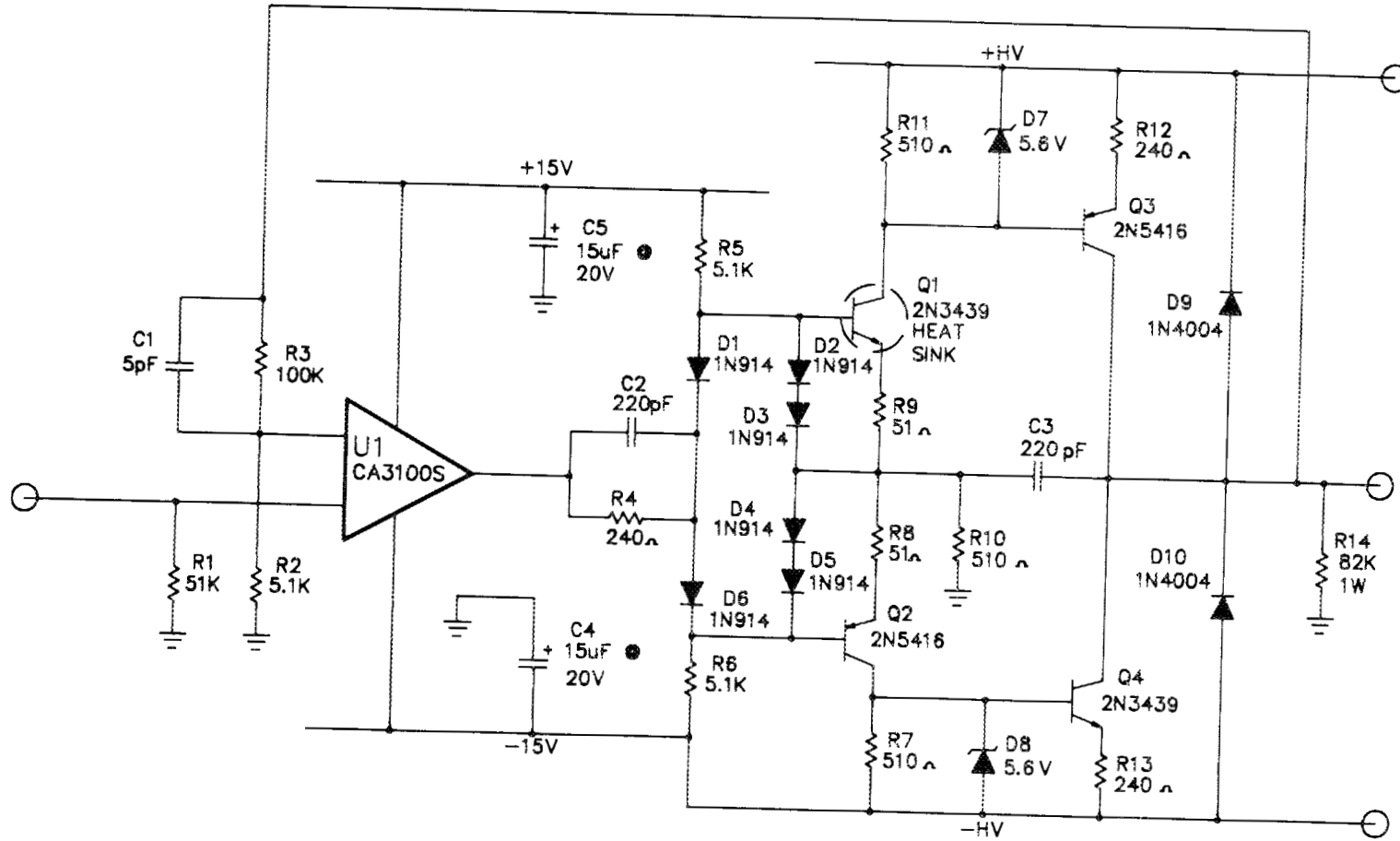


Fig. 9. High voltage operational amplifier schematic diagram.

### 3.7 Valve Drive Gate

Since the system is designed to be essentially unattended, it is quite probable that it would be left on with no operator present. In the event of a circuit fault, the valve could be driven open and the entire Tokamak could rise to atmospheric or greater pressure. Such an occurrence would render the experiment inoperative for at least 24 h and, for some gases, could result in a delay of a week or more.

An output drive gate which uses a monostable multivibrator circuit and two relays was designed to complete the path from the high-voltage operational amplifier ( $A_1$  of Fig. 1 and Fig. 9) to the gas valve (Fig. 2) for a 2-s interval and is triggered by a timing pulse from the control room computer. A switch is provided to override the gate manually during testing. The schematic for the gate is shown in Fig. 10.

### 3.8 System Overview

The simplified diagram in Fig. 1 shows an overview of the whole system and illustrates how the components interact. Detailed analysis and nominal simulation of system response follow in Sect. 4.

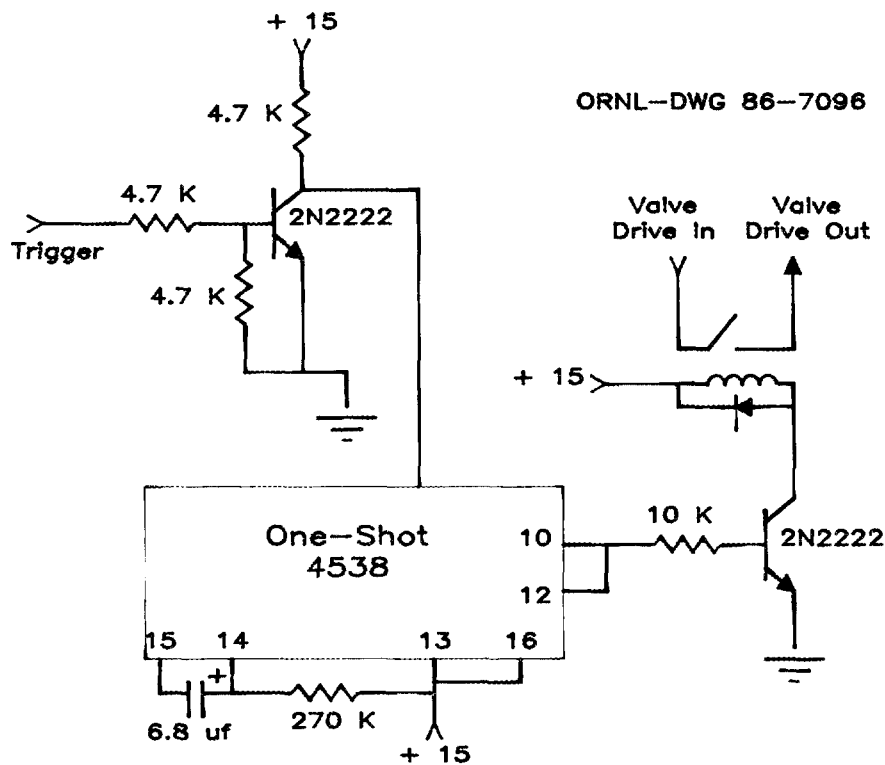


Fig. 10. Valve drive gate schematic diagram.

## 4. ANALYSIS OF SYSTEM COMPONENTS AND RESPONSE

The IBM CSMP III program has been chosen to model this system because of its flexibility and its ability to mix differential equations and Laplace transforms in the same model. This feature is particularly convenient to the simulation of this system. Since detailed modeling of electronic circuits is not practical with this program, macromodels will be used, employing manually derived transfer functions. A state-variable model of the gas injector is used employing the differential equation described in Sect. 2 and using hardware characterizations from the manufacturer's data as well as from empirical observations.

Three circuit configurations have been employed to develop macromodels for this system. Two are the familiar shunt and series feedback circuits, while the third is a series feedback configuration which has a dynamic impedance in the feedback voltage divider. The series case shown in Fig. 11 is modeled by the familiar equation<sup>5</sup>

$$\frac{A_{ol}}{1 + A_{ol}B} \quad (4)$$

ORNL-DWG 86-7097

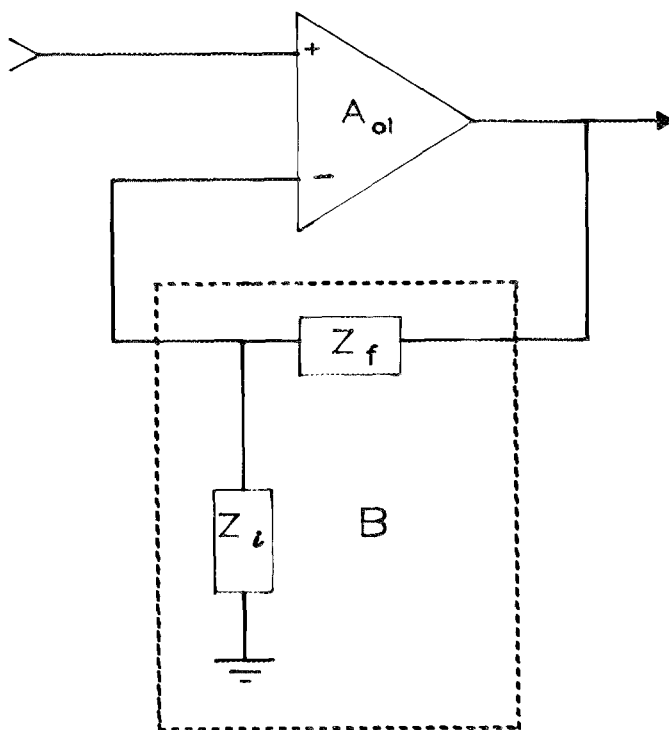


Fig. 11. General configuration of a series feedback amplifier.

For frequencies of interest in this system, the amplifier's input impedance is approximated as infinite. The manufacturer's data for the operational amplifiers employed indicate well behaved, dominant pole compensation. The operational amplifiers themselves may, therefore, be modeled as

$$\frac{G}{\tau_b S + 1} ,$$

where  $G$  is the small signal dc open loop gain, and

$$\tau_b = \frac{1}{2\pi f_b} ,$$

where  $f_b$  is the high-frequency, 3-dB value for the open loop gain. For the series feedback amplifier then

$$A_{CL} = \frac{\frac{G}{\tau_b S + 1}}{1 + \frac{GB}{\tau_b S + 1}} ,$$

which may be written as

$$\frac{G}{GB + \tau_b S + 1} . \quad (5)$$

Factoring gives

$$A_{CL} = \frac{G}{GB + 1} \times \frac{1}{\frac{\tau_b}{GB + 1} S + 1} ,$$

which is a convenient form when  $B$  is a real number. In the simple case of a unity-gain voltage follower, this form reduces to

$$\frac{1}{\frac{\tau_b}{G} S + 1} .$$

The line receiver of Fig. 8 operates at a gain of 10 with an input divider gain of 0.10 to provide additional common mode range. The capacitors are adjusted so that the ac division ratios are the same as the dc ratios with no visible overshoot. This adjustment simplifies the analysis substantially in that the only remaining frequency dependence in the circuit is the operational amplifier gain and the input impedance, which is still considered negligible for the frequencies of interest. As shown in Fig. 8, the closed-loop gain of the line receiver is

$$\frac{1}{\frac{\tau_b}{G \times B + 1} S + 1} = \frac{1}{\frac{6.25 \times 10^{-3}}{1.8 \times 10^5} S + 1} ,$$

since  $B = 0.10$ , and, for the LF 356,  $\tau_b = 6.25 \times 10^{-3}$  and  $G = 1.8 \times 10^5$ . Thus, the above gain equation reduces to

$$\frac{1}{3.819 \times 10^{-7} S + 1}$$

for the National Semiconductor LF 356.

The high-voltage operational amplifier in Fig. 9 uses series feedback in a single-pole, low-pass filter configuration. As illustrated in Figs. 9 and 11,  $B$  may be written as

$$R_2 + \frac{\frac{R_2}{R_3} \frac{1}{SC_1}}{R_3 + \frac{1}{SC_1}} ,$$

which may be simplified to

$$\frac{R_2 R_3 C_1 S + R_2}{R_2 R_3 C_1 S + R_2 + R_3} .$$

For the RCA CA3100S,  $G$  is  $1 \times 10^3$  and  $\tau_b$  is  $1.45 \times 10^{-6}$ . Substituting these values into Eq. 5 and rearranging the denominator yields

$$A_{CL} = \frac{10^3}{1.45 \times 10^{-6} S + \frac{2.55 S + 5.1 \times 10^6}{2.55 \times 10^{-3} S + 105,100} + 1} ,$$

which simplifies to

$$20.192 \times \frac{2.426 \times 10^{-8} S + 1}{1.032 \times 10^{-14} S^2 + 5.1967 \times 10^{-7} S + 1} .$$

An interesting application of series feedback occurs in the transducer preamplifier circuit where a dynamic impedance appears in series with the feedback voltage divider. Analysis is facilitated by invoking Miller's Theorem.<sup>5</sup> Referring to Fig. 12 from Miller's Theorem,

$$Z_i = \frac{Z_f}{(1 - A)} .$$

ORNL-DWG 86-7098

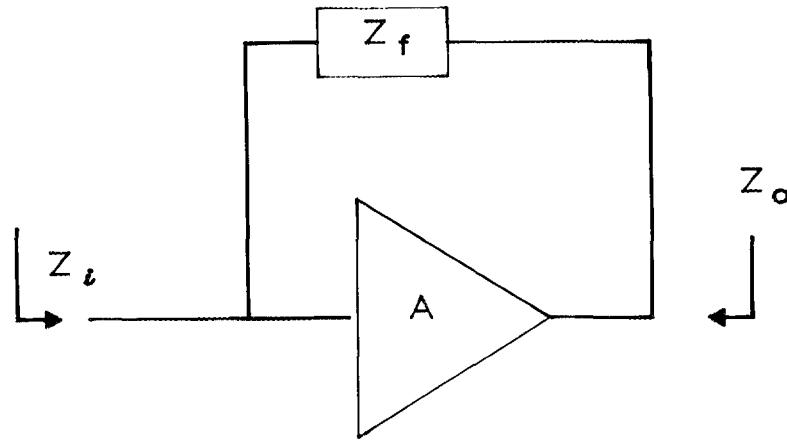


Fig. 12. Feedback diagram for Miller's Theorem.

As shown in Fig. 6, the closed-loop gain of the preamplifier input stage may be written employing Eq. 4 and is given by

$$A_{CL} = \frac{A_{ol}}{1 + A_{ol} \frac{R_4 + \frac{R_5}{A_{ol} + 1}}{R_3 + R_4 + \frac{R_5}{A_{ol} + 1}}}$$

Noting that  $R_5 = R_3$ , making the substitution while using the previously defined notation for operational amplifier gain, and assuming that  $A_{ol}$  is large compared to one, this expression may be expanded to

$$\begin{aligned} & \frac{G(R_3 + R_4) + R_3}{GR_4 + 2R_3 + R_4 + \frac{R_3}{G}} \\ & \times \frac{\frac{R_3 \tau_b}{G(R_3 + R_4) + R_3} S + 1}{\frac{R_3 \tau_b^2}{G^2 R_4 + G(2R_3 + R_4) + R_3} S^2 + \frac{\tau_b (2R_3 + R_4 + \frac{2R_3}{G})}{(G + 1)R_4 + 2R_3 + \frac{R_3}{G}} S + 1} \end{aligned}$$

For Precision Monolithics Model OP-07 ( $U_4$  and  $U_5$  of Fig. 6),  $G = 5 \times 10^5$  and  $\tau_b = 8 \times 10^{-2}$ . Inserting the numbers and simplifying gives

$$A_{CL} = 20.998 \times \frac{1.52 \times 10^{-7}S + 1}{5.12 \times 10^{-13}S^2 + 6.56 \times 10^{-6}S + 1}$$

The final amplifier configuration of interest is the shunt feedback case. This case has two signal components, the parasitic gain of the feedback circuit and the amplifier active gain. The circuit configuration is shown in Fig. 13. The passive gain circuit is shown in Fig. 14, from which the passive gain is written

$$\frac{V_o}{V_i}_{\text{Passive}} = \frac{R_o}{R_o + Z_f + Z_i}$$

Since the parasitic gain term is<sup>5</sup>

$$\frac{\text{Passive Gain}}{1 + T}$$

the parasitic gain is then

$$\frac{\frac{R_o}{R_o + Z_f + Z_i}}{1 + T} = \frac{\frac{R_o}{Z_o + Z_f + Z_i}}{1 + \frac{A_{ol}(Z_i)}{R_o + Z_f + Z_i}}$$

which reduces to

$$\frac{R_o}{A_{ol}Z_i + R_o + Z_f + Z_i} \quad (6)$$

Using the previous notation for operational amplifier gain, this expression may be written in the form

$$\frac{R_o}{R_o + R_f + R_i + GR_i} \times \frac{\tau_b S + 1}{\frac{\tau_b(R_o + R_f + R_i)}{GR_i + R_o + R_f + R_i} S + 1}$$

Substituting appropriate numbers for  $U_6$  in the preamplifier circuit yields a forward parasitic gain of

$$5.566 \times 10^{-7} \times \frac{2 \times 10^{-3}S + 1}{2.3486 \times 10^{-7}S + 1}$$

for the National Semiconductor LF357, in which  $G = 1.8 \times 10^5$ ,  $\tau_b = 2 \times 10^{-3}$ , and  $R_o \approx 50 \Omega$ .

ORNL-DWG 86-7099

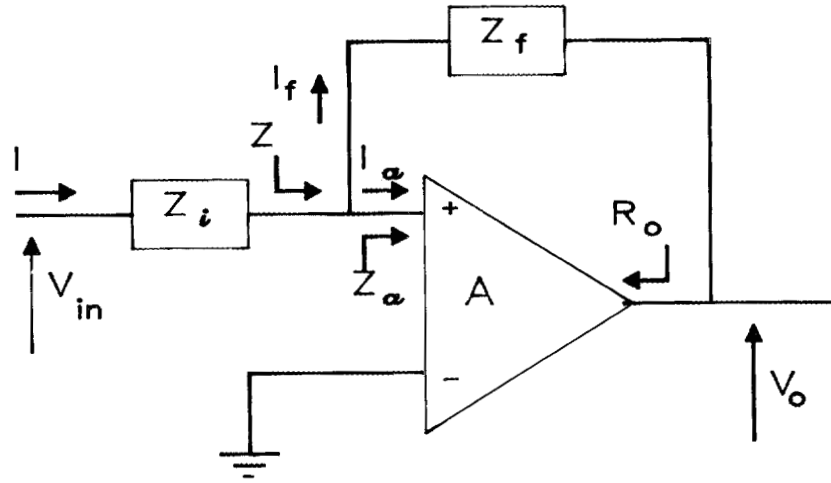


Fig. 13. General configuration of a shunt feedback amplifier.

ORNL-DWG 86-7100

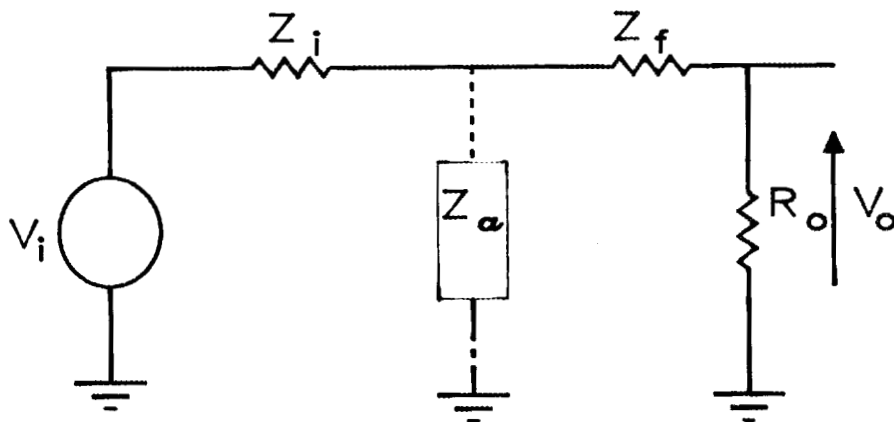


Fig. 14. Passive gain CKT of shunt feedback amplifier.

The active gain of the shunt feedback amplifier is developed from Fig. 13. The analysis is greatly facilitated by the application of Miller's Theorem. Referring to Fig. 13,  $V_o$  may be written as

$$V_o = V_{in} - IZ_i - I_f Z_f ,$$

invoking Miller's Theorem,

$$Z = \frac{Z_f}{(1 - A)} // Z_a ,$$

and

$$I = \frac{V_{in}}{Z_i + \frac{Z_f}{1 + A} // Z_a} .$$

By current division,

$$\frac{I_f}{I} = \frac{Z_a}{\frac{Z_f}{1 + A} + Z_a} .$$

Substituting and factoring yields

$$\frac{V_o}{V_{in}} = 1 - \frac{Z_i}{Z_i + \frac{Z_f}{1 + A} // Z_a} \cdot \frac{Z_a Z_f}{Z_i \frac{Z_f}{1 + A} // Z_a \left( \frac{Z_f}{1 + A} + Z_a \right)} .$$

With some algebra this may be rewritten as

$$\frac{V_o}{V_{in}} = 1 - \frac{Z_i}{Z_i + \frac{Z_f}{1 + A} // Z_a} \left( 1 + \frac{Z_f}{Z_i} \frac{Z_a}{\frac{Z_f}{1 + A} + Z_a} \right) . \quad (7)$$

For frequencies of interest in this system,  $Z_a$  is negligible, hence the expression reduces to

$$1 - \frac{Z_i + Z_f}{Z_i + \frac{Z_f}{1 + A}} = \frac{\frac{Z_f}{1 + A} - Z_f}{Z_i + \frac{Z_f}{1 + A}} .$$

When  $Z_f$  and  $Z_i$  are real and the amplifier response is characterized as

$$\frac{G}{\tau_b S + 1} ,$$

simplification and factoring yields

$$\frac{V_o}{V_{in}} = \frac{-GR_f}{GR_i + R_f + R_i} \times \frac{1}{\frac{\tau_b(R_f + R_i)}{GR_i + R_f + R_i} S + 1} \quad (8)$$

Inserting appropriate numbers for  $U_7$  of the preamplifier circuit, the active gain may be written

$$-20.03774 \times \frac{1}{2.3375 \times 10^{-7} S + 1}$$

The total gain of the inverting path is therefore

$$\frac{5.566 \times 10^{-7} (2 \times 10^{-3} S + 1)}{2.3486 \times 10^{-7} S + 1} - \frac{20.03774}{2.3375 \times 10^{-7} S + 1}$$

The gain of the noninverting side of this differential amplifier is adjusted with  $R_7$  to match precisely the corresponding gain of the inverting side. Hence, the active gain is matched in magnitude and frequency response to the gain of the inverting amplifier. Examination of the equations reveals that high-frequency common mode rejection of the preamplifier is hampered by the parasitic forward gain of the inverting half of the differential amplifier. In operation, no problems related to high-frequency common mode rejection were encountered.

The error amplifier of Fig. 7 is a shunt feedback amplifier with a nominal gain of 10. Employing the parasitic gain formula (Eq. 6) in expanded form,

$$A_p = \frac{R_o}{R_o + R_f + R_i + GR_i} \times \frac{\tau_b S + 1}{\frac{\tau_b(R_o + R_f + R_i)}{GR_i + R_o + R_f + R_i} S + 1},$$

and referring to Fig. 7, the parasitic gain of the error amplifier ( $U_2$ ) may be written as

$$\frac{50}{50 + R_7 + R_8 + R_6 + 1.8 \times 10^5 R_6} \times \frac{6.25 \times 10^{-3} S + 1}{\frac{6.25 \times 10^{-3} (50 + R_7 + R_8 + R_6)}{1.8 \times 10^5 R_6 + 50 + R_7 + R_8 + R_6} S + 1}$$

Substituting circuit values gives

$$2.78 \times 10^{-8} \times \frac{6.25 \times 10^{-3}S + 1}{1.222 \times 10^{-6}S + 1} .$$

The active gain of the error amplifier ( $U_2$ ) circuit is obtained by employing Eq. 8 and is given by

$$\frac{-1.8 \times 10^5(R_7 + R_8)}{1.8 \times 10^5 R_6 + R_7 + R_8 + R_6} \times \frac{1}{\frac{6.25 \times 10^{-3}(R_7 + R_8 + R_6)}{1.8 \times 10^5 R_6 + R_7 + R_8 + R_6} S + 1} .$$

With constants for the error amplifier circuit substituted, the active gain is

$$-9.999 \times \frac{1}{1.222 \times 10^{-6}S + 1} .$$

Thus the electronic subassemblies of the system have been modeled in a form compatible with the CSMP program. The subassemblies with their respective transfer functions have been depicted in the system block diagram from which the modeling program was written.

The final subsystem to be modeled is the gas valve and gas-injector assembly. Burrell's original work has been relied upon to determine appropriate constants for the model of this subsystem. Equation 2 gives the differential density at the top of the injector tube as a function of the flow entering and leaving the injector. Equation 2 is given by

$$\frac{d}{dt} PV = -CP^2 + Q(t) .$$

Since  $V$  is constant, we can rearrange the equation and write

$$\dot{P} = \frac{1}{V} [-CP^2 + Q(t)] .$$

This form of the differential equation allows convenient modeling by CSMP III, since one need only define  $V$ ,  $C$ , and a function which will give the imposed flow. Recalling (from Eq. 1) that

$$C = \frac{\pi a^4}{16\eta l} ,$$

then multiplying by the conversion factor of

$$1333.224 \frac{\frac{\text{dynes}}{\text{cm}^2}}{\text{torr}} ,$$

and using measured values of  $a = 0.357$  mm,  $l = 75.2$  cm, and  $\eta = 87.6 \times 10^{-6}$  poise,  $C$  becomes<sup>1</sup>

$$6.45 \times 10^{-5} \frac{\text{L}}{\text{torr} \cdot \text{s}} .$$

In the special case of no imposed flow, Eq. 3 has the pressure related by

$$P(t) = \frac{P_0}{1 + \frac{C}{V} P_0 t} ,$$

where  $P_0$  is the pressure at  $t = 0$ .

Burrell's solution under the same conditions was<sup>1</sup>

$$\frac{1}{P(t)} = \frac{1}{P_0} + B(t - t_0) .$$

Rearranging with  $t_0 = 0$  gives

$$P(t) = \frac{P_0}{1 + P_0 B t} .$$

Thus,

$$B = \frac{C}{V}$$

and

$$V = \frac{C}{B} .$$

Burrell measured a value of<sup>1</sup>

$$1.2 \times 10^{-4} \frac{\text{cm}^2}{\text{dyne} \cdot \text{s}} \text{ for } B .$$

Converting to torr gives

$$B = \frac{0.1599}{\text{torr} \cdot \text{s}}$$

from which

$$V = \frac{\frac{6.45 \times 10^{-5} \text{ L}}{\text{torr} \cdot \text{s}}}{\frac{0.1599}{\text{torr} \cdot \text{s}}} = 4.03 \times 10^{-4} \text{ L} .$$

There are conflicting data on the maximum throughput of the piezoelectric valve. The manufacturer's data indicate a maximum throughput of about 10 torr-L/s, while Burrell has measured throughput of 41 torr-L/s.<sup>1</sup> Once the valve opens, the throughput is approximately a linear function of the applied voltage and the pressure across the valve (see Fig. 2); hence,

$$Q = kV(P_{in} - P_{out}) \quad ,$$

where  $k$  is the proportionality constant,  $V$  is the valve drive voltage from the high-voltage operational amplifier,  $P_{in}$  is the gas source pressure, and  $P_{out}$  is the gas pressure downstream of the valve. The value of  $k$  was determined so that 45 torr-L/s would flow when the pressure drop across the valve was 760 torr and the valve drive was 120 V. This value allows a 30-V dead band in the valve. Thus,  $k$  is  $4.934 \times 10^{-6}$ .

The final element in the injector is the pressure transducer, which has an output of 2 mV/psia or 38.68  $\mu$ V/torr.

Thus, each element of the system is now modeled sufficiently to allow computer simulation of the system response.

A detailed block diagram for the entire system is given in Fig. 15. The auto-zero circuit in the preamplifier, the valve popping circuit in the error amplifier, and the valve drive gate have been omitted because they do not affect system response or stability and would add unnecessary complexity to the CSMP program.

CSMP III<sup>6</sup> was used to model the system's temporal response to both step and sawtooth demand functions.

The system block diagram (Fig. 15) interprets the variables on all computer simulation plots. Figure 16 depicts the response of the valve and injector system alone to a 150-ms-wide pulse beginning 10 ms into the simulation. From the simulation output plot, the 10 to 90% rise time of the flow is approximately 20 ms, and after the imposed flow is removed, the pressure is observed to decline proportionally to  $1/t$ , while the flow declines as  $1/t^2$ . Reference to Fig. 16 and the transfer functions of the electronic modules suggests that the dynamic response of the gas injector and valve constitutes the system's dominant pole.

Figure 17 simulates the closed-loop system response to a 10-V demand signal during the initial 40 ms of flow. Here the rise time to 5.8 torr-L/s has been reduced to about 3.5 ms by the closed-loop system opening the gas valve fully until the steady-state flow is established.

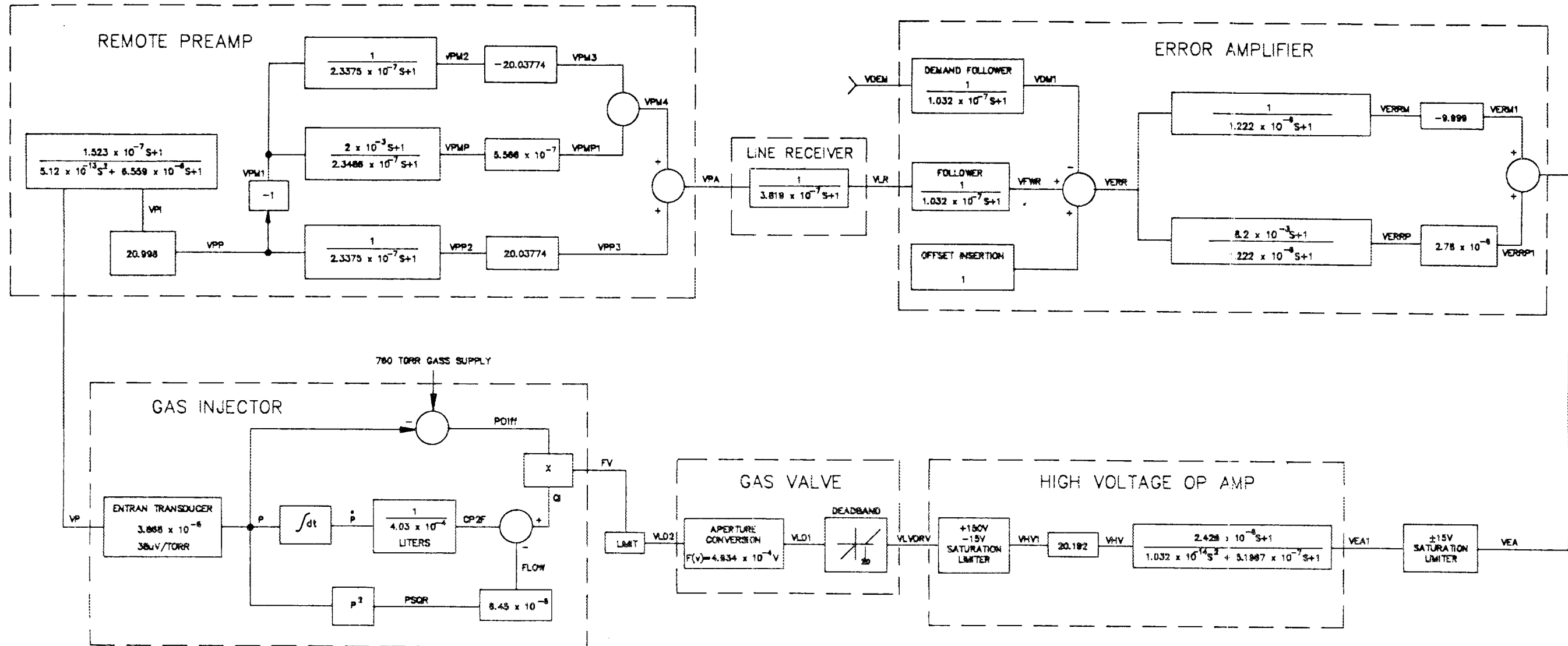


Fig. 15. Detailed system block diagram.

5

TIME	FV							P	FLOW	PDIF				
.0	.0	*	-----I-----I-----I-----0-----X					.0	.0	760.00				
2.0000E-02	2.0000E-02	I		0	I	X	*	I	+	258.22	-4.3006	501.78		
4.0000E-02	2.0000E-02	IO		X	I			I	*	+	350.50	-7.9239	409.50	
6.0000E-02	2.0000E-02	0		X	I			I	*	+	354.41	-8.1015	405.59	
8.0000E-02	2.0000E-02	0		X	I			I	*	+	354.56	-8.1084	405.44	
.10000	2.0000E-02	0		X	I			I	*	+	354.56	-8.1087	405.44	
.12000	2.0000E-02	0		X	I			I	*	+	354.56	-8.1087	405.44	
.14000	2.0000E-02	0		X	I			I	*	+	354.56	-8.1087	405.44	
.16000	2.0000E-02	0		X	I			I	*	+	354.56	-8.1087	405.44	
.18000	.0	+			I	*	0I		I	X	I	166.08	-1.7791	593.92
.20000	.0	+	-----I*-----I-----0-----X-----I									108.44	-7.5841	651.56
.22000	.0	+		*	I			0	I	X	I	80.495	-4.1793	679.50
.24000	.0	+		*	I			0	X	I		64.004	-2.26422	696.00
.26000	.0	+		*	I			IO	X	I		53.121	-1.18201	706.88
.28000	.0	+		*	I			I	0	X		45.401	-1.13295	714.60
.30000	.0	+		*	I			I	0	X		39.640	-1.10135	720.36
.32000	.0	+		*	I			I	0	X		35.177	-7.9812E-02	724.82
.34000	.0	+		*	I			I	0	X		31.617	-6.4475E-02	728.38
.36000	.0	+		*	I			I	0	X		28.711	-5.3168E-02	731.29
.38000	.0	+		*	I			I	0	X		26.294	-4.4595E-02	733.71
.40000	.0	+	-----I-----I-----I-----0-----X									24.253	-3.7939E-02	735.75
.42000	.0	+		*	I			I	0	X		22.506	-3.2670E-02	737.49
.44000	.0	+		*	I			I	0	X		20.993	-2.8427E-02	739.01
.46000	.0	+		*	I			I	0	X		19.671	-2.4959E-02	740.33
.48000	.0	+		*	I			I	0	X		18.506	-2.2090E-02	741.49
.50000	.0	+		*	I			I	0	X		17.471	-1.9688E-02	742.53
.52000	.0	+		*	I			I	0	X		16.546	-1.7658E-02	743.45
.54000	.0	+		*	I			I	0	X		15.714	-1.5926E-02	744.29
.56000	.0	+		*	I			I	0	X		14.961	-1.4437E-02	745.04
.58000	.0	+		*	I			I	0	X		14.277	-1.3148E-02	745.72
.60000	.0	+	-----I-----I-----I-----0-----X									13.653	-1.2024E-02	746.35
.62000	.0	++			I			I	0	X		13.082	-1.1038E-02	746.92
.64000	.0	++			I			I	0	X		12.556	-1.0168E-02	747.44
.66000	.0	++			I			I	0	X		12.071	-9.3978E-03	747.93
.68000	.0	++			I			I	0	X		11.622	-8.7116E-03	748.38
.70000	.0	++			I			I	0	X		11.205	-8.0979E-03	748.80
.72000	.0	++			I			I	0	X		10.817	-7.5468E-03	749.18
.74000	.0	++			I			I	0	X		10.455	-7.0501E-03	749.54
.76000	.0	++			I			I	0	X		10.116	-6.6009E-03	749.88
.78000	.0	++			I			I	0	X		9.7990	-6.1933E-03	750.20
.80000	.0	++	-----I-----I-----I-----0-----X									9.5010	-5.8223E-03	750.50
.82000	.0	++			I			I	0	X		9.2206	-5.4837E-03	750.78
.84000	.0	++			I			I	0	X		8.9562	-5.1738E-03	751.04
.86000	.0	++			I			I	0	X		8.7066	-4.8894E-03	751.29
.88000	.0	++			I			I	0	X		8.4705	-4.6279E-03	751.53
.90000	.0	++			I			I	0	X		8.2469	-4.3868E-03	751.75
.92000	.0	++			I			I	0	X		8.0348	-4.1640E-03	751.97
.94000	.0	++			I			I	0	X		7.8334	-3.9578E-03	752.17
.96000	.0	++			I			I	0	X		7.6417	-3.7666E-03	752.36
.98000	.0	++			I			I	0	X		7.4593	-3.5888E-03	752.54
1.0000	.0	++	-----I-----I-----I-----0-----X									7.2853	-3.4234E-03	752.71

Fig. 16. CSMP III simulation of gas injector open-loop pulse response.

TIME	VDM1	X	*	+	VFWR	FLOW
.0	.0	X			.0	.0
8.0000E-04	.0	X			.0	.0
1.6000E-03	.0	X			.0	.0
2.4000E-03	.0	X			.0	.0
3.2000E-03	.0	X			.0	.0
4.0000E-03	.0	X			.0	.0
4.8000E-03	.0	X			.0	.0
5.6000E-03	10.000	I X	*	I	+ 2.0827	.26417
6.4000E-03	10.000	I	X	I	+ 4.5505	1.2611
7.2000E-03	10.000	I		I	+ 6.6684	2.7081
8.0000E-03	10.000	I		I	+ 8.4560	4.3546
8.8000E-03	10.000	I		I	X * + 9.6584	5.6810
9.6000E-03	10.000	I		I	X++ 9.7676	5.8102
1.0400E-02	10.000	I		I	X++ 9.7725	5.8161
1.1200E-02	10.000	I		I	X++ 9.7729	5.8165
1.2000E-02	10.000	I		I	X++ 9.7729	5.8165
1.2800E-02	10.000	I		I	X++ 9.7729	5.8165
1.3600E-02	10.000	I		I	X++ 9.7729	5.8165
1.4400E-02	10.000	I		I	X++ 9.7729	5.8165
1.5200E-02	10.000	I		I	X++ 9.7729	5.8165
1.6000E-02	10.000	I		I	X++ 9.7729	5.8165
1.6800E-02	10.000	I		I	X++ 9.7729	5.8165
1.7600E-02	10.000	I		I	X++ 9.7729	5.8165
1.8400E-02	10.000	I		I	X++ 9.7729	5.8165
1.9200E-02	10.000	I		I	X++ 9.7729	5.8165
2.0000E-02	10.000	I		I	X++ 9.7729	5.8165
2.0800E-02	10.000	I		I	X++ 9.7729	5.8165
2.1600E-02	10.000	I		I	X++ 9.7729	5.8165
2.2400E-02	10.000	I		I	X++ 9.7729	5.8165
2.3200E-02	10.000	I		I	X++ 9.7729	5.8165
2.4000E-02	10.000	I		I	X++ 9.7729	5.8165
2.4800E-02	10.000	I		I	X++ 9.7729	5.8165
2.5600E-02	10.000	I		I	X++ 9.7729	5.8165
2.6400E-02	10.000	I		I	X++ 9.7729	5.8165
2.7200E-02	10.000	I		I	X++ 9.7729	5.8165
2.8000E-02	10.000	I		I	X++ 9.7729	5.8165
2.8800E-02	10.000	I		I	X++ 9.7729	5.8165
2.9600E-02	10.000	I		I	X++ 9.7729	5.8165
3.0400E-02	10.000	I		I	X++ 9.7729	5.8165
3.1200E-02	10.000	I		I	X++ 9.7729	5.8165
3.2000E-02	10.000	I		I	X++ 9.7729	5.8165
3.2800E-02	10.000	I		I	X++ 9.7729	5.8165
3.3600E-02	10.000	I		I	X++ 9.7729	5.8165
3.4400E-02	10.000	I		I	X++ 9.7729	5.8165
3.5200E-02	10.000	I		I	X++ 9.7729	5.8165
3.6000E-02	10.000	I		I	X++ 9.7729	5.8165
3.6800E-02	10.000	I		I	X++ 9.7729	5.8165
3.7600E-02	10.000	I		I	X++ 9.7729	5.8165
3.8400E-02	10.000	I		I	X++ 9.7729	5.8165
3.9200E-02	10.000	I		I	X++ 9.7729	5.8165
4.0000E-02	10.000	I		I	X++ 9.7729	5.8165

(A) Plot of flow in torr-liters/second, pressure feedback signal and demand signal in volts.

Fig. 17. CSMP III simulation of closed-loop system rise time.

TIME	VDMI					VERR	VEA	VLVDRV	
.0	.0					.10000	-1.0000	-15.000	
8.0000E-04	.0	+	0 X I	I	I*	I .10000	-1.0000	-15.000	
1.6000E-03	.0	+	0 X I	I	I*	I .10000	-1.0000	-15.000	
2.4000E-03	.0	+	0 X I	I	I*	I .10000	-1.0000	-15.000	
3.2000E-03	.0	+	0 X I	I	I*	I .10000	-1.0000	-15.000	
4.0000E-03	.0	+	0 X I	I	I*	I .10000	-1.0000	-15.000	
4.8000E-03	.0	+	0 X I	I	I*	I .10000	-1.0000	-15.000	
5.6000E-03	10.000	I	*	I	I	X 0 -7.8173	16.000	150.00	
6.4000E-03	10.000	I		I *	I	X 0 -5.3495	16.000	150.00	
7.2000E-03	10.000	I		I	*I	I X 0 -3.2316	16.000	150.00	
8.0000E-03	10.000	I				-1.4440	14.440	150.00	
8.8000E-03	10.000	I		I X	0	*I	+ -.24161	2.4161	48.805
9.6000E-03	10.000	I		I X	0	I	+ -.13241	1.3241	26.748
1.0400E-02	10.000	I		I X	0	I	+ -.12745	1.2745	25.746
1.1200E-02	10.000	I		I X	0	I	+ -.12708	1.2708	25.671
1.2000E-02	10.000	I		I X	0	I	+ -.12706	1.2706	25.666
1.2800E-02	10.000	I		I X	0	I	+ -.12706	1.2706	25.666
1.3600E-02	10.000	I		I X	0	I	+ -.12706	1.2706	25.666
1.4400E-02	10.000	I		I X	0	I	+ -.12706	1.2706	25.666
1.5200E-02	10.000	I		I X	0	I	+ -.12706	1.2706	25.666
1.6000E-02	10.000	I		I X	0	I	+ -.12706	1.2706	25.666
1.6800E-02	10.000	I		I X	0	I	+ -.12706	1.2706	25.666
1.7600E-02	10.000	I		I X	0	I	+ -.12706	1.2706	25.666
1.8400E-02	10.000	I		I X	0	I	+ -.12706	1.2706	25.666
1.9200E-02	10.000	I		I X	0	I	+ -.12706	1.2706	25.666
2.0000E-02	10.000	I		I X	0	I	+ -.12706	1.2706	25.666
2.0800E-02	10.000	I		I X	0	I	+ -.12706	1.2706	25.666
2.1600E-02	10.000	I		I X	0	I	+ -.12706	1.2706	25.666
2.2400E-02	10.000	I		I X	0	I	+ -.12706	1.2706	25.666
2.3200E-02	10.000	I		I X	0	I	+ -.12706	1.2706	25.666
2.4000E-02	10.000	I		I X	0	I	+ -.12706	1.2706	25.666
2.4800E-02	10.000	I		I X	0	I	+ -.12706	1.2706	25.666
2.5600E-02	10.000	I		I X	0	I	+ -.12706	1.2706	25.666
2.6400E-02	10.000	I		I X	0	I	+ -.12706	1.2706	25.666
2.7200E-02	10.000	I		I X	0	I	+ -.12706	1.2706	25.666
2.8000E-02	10.000	I		I X	0	I	+ -.12706	1.2706	25.666
2.8800E-02	10.000	I		I X	0	I	+ -.12706	1.2706	25.666
2.9600E-02	10.000	I		I X	0	I	+ -.12706	1.2706	25.666
3.0400E-02	10.000	I		I X	0	I	+ -.12706	1.2706	25.666
3.1200E-02	10.000	I		I X	0	I	+ -.12706	1.2706	25.666
3.2000E-02	10.000	I		I X	0	I	+ -.12706	1.2706	25.666
3.2800E-02	10.000	I		I X	0	I	+ -.12706	1.2706	25.666
3.3600E-02	10.000	I		I X	0	I	+ -.12706	1.2706	25.666
3.4400E-02	10.000	I		I X	0	I	+ -.12706	1.2706	25.666
3.5200E-02	10.000	I		I X	0	I	+ -.12706	1.2706	25.666
3.6000E-02	10.000	I		I X	0	I	+ -.12706	1.2706	25.666
3.6800E-02	10.000	I		I X	0	I	+ -.12706	1.2706	25.666
3.7600E-02	10.000	I		I X	0	I	+ -.12706	1.2706	25.666
3.8400E-02	10.000	I		I X	0	I	+ -.12706	1.2706	25.666
3.9200E-02	10.000	I		I X	0	I	+ -.12706	1.2706	25.666
4.0000E-02	10.000	I		I X	0	I	+ -.12706	1.2706	25.666

(B) Plot of valve drive, error amplifier output and input, and demand signals in volts.

Fig. 17 (continued)

TIME	PDOT	'X'=VDM1	'#'=FLOW	'+'=PDOT	10.00	6.000	1.200E+05	FLOW	VDM1
.0	.0	X	-----	-----	-----	I	.0	.0	.0
8.0000E-04	.0	X	I	I	I	I	.0	.0	.0
1.6000E-03	.0	X	I	I	I	I	.0	.0	.0
2.4000E-03	.0	X	I	I	I	I	.0	.0	.0
3.2000E-03	.0	X	I	I	I	I	.0	.0	.0
4.0000E-03	.0	X	I	I	I	I	.0	.0	.0
4.8000E-03	.0	X	I	I	I	I	.0	.0	.0
5.6000E-03	1.0160E+05	I	*	I	I	*	X	.26417	10.000
6.4000E-03	87989.	I	*	I	I	+I	X	1.2611	10.000
7.2000E-03	74836.	I		I	*	I	X	2.7081	10.000
8.0000E-03	62681.	I	-----	-----	-----	-----	X	4.3546	10.000
8.8000E-03	13559.	I	+	I	I	I	* X	5.6810	10.000
9.6000E-03	630.03	+	I	I	I	I	* X	5.8102	10.000
1.0400E-02	47.040	+	I	I	I	I	* X	5.8161	10.000
1.1200E-02	3.2207	+	I	I	I	I	* X	5.8165	10.000
1.2000E-02	.63421	+	I	I	I	I	* X	5.8165	10.000
1.2800E-02	.63421	+	I	I	I	I	* X	5.8165	10.000
1.3600E-02	.63421	+	I	I	I	I	* X	5.8165	10.000
1.4400E-02	.63421	+	I	I	I	I	* X	5.8165	10.000
1.5200E-02	.63421	+	I	I	I	I	* X	5.8165	10.000
1.6000E-02	.63421	+	-----	-----	-----	-----	* X	5.8165	10.000
1.6800E-02	.63421	+	I	I	I	I	* X	5.8165	10.000
1.7600E-02	.63421	+	I	I	I	I	* X	5.8165	10.000
1.8400E-02	.63421	+	I	I	I	I	* X	5.8165	10.000
1.9200E-02	.63421	+	I	I	I	I	* X	5.8165	10.000
2.0000E-02	.63421	+	I	I	I	I	* X	5.8165	10.000
2.0800E-02	.63421	+	I	I	I	I	* X	5.8165	10.000
2.1600E-02	.63421	+	I	I	I	I	* X	5.8165	10.000
2.2400E-02	.63421	+	I	I	I	I	* X	5.8165	10.000
2.3200E-02	.63421	+	I	I	I	I	* X	5.8165	10.000
2.4000E-02	.63421	+	-----	-----	-----	-----	* X	5.8165	10.000
2.4800E-02	.63421	+	I	I	I	I	* X	5.8165	10.000
2.5600E-02	.63421	+	I	I	I	I	* X	5.8165	10.000
2.6400E-02	.63421	+	I	I	I	I	* X	5.8165	10.000
2.7200E-02	.63421	+	I	I	I	I	* X	5.8165	10.000
2.8000E-02	.63421	+	I	I	I	I	* X	5.8165	10.000
2.8800E-02	.63421	+	I	I	I	I	* X	5.8165	10.000
2.9600E-02	.63421	+	I	I	I	I	* X	5.8165	10.000
3.0400E-02	.63421	+	I	I	I	I	* X	5.8165	10.000
3.1200E-02	.63421	+	I	I	I	I	* X	5.8165	10.000
3.2000E-02	.63421	+	-----	-----	-----	-----	* X	5.8165	10.000
3.2800E-02	.63421	+	I	I	I	I	* X	5.8165	10.000
3.3600E-02	.63421	+	I	I	I	I	* X	5.8165	10.000
3.4400E-02	.63421	+	I	I	I	I	* X	5.8165	10.000
3.5200E-02	.63421	+	I	I	I	I	* X	5.8165	10.000
3.6000E-02	.63421	+	I	I	I	I	* X	5.8165	10.000
3.6800E-02	.63421	+	I	I	I	I	* X	5.8165	10.000
3.7600E-02	.63421	+	I	I	I	I	* X	5.8165	10.000
3.8400E-02	.63421	+	I	I	I	I	* X	5.8165	10.000
3.9200E-02	.63421	+	I	I	I	I	* X	5.8165	10.000
4.0000E-02	.63421	+	-----	-----	-----	-----	* X	5.8165	10.000

(C) Plot of demand in volts, flow in torr-liters/second, and  $dP/dt$  in torrs/second squared.

Fig. 17 (continued)

Figure 18 is a 1-s simulation of the closed-loop response to a 150-ms, 10-V demand pulse. Because the imposed flow is unipolar, feedback does not affect the decay time. For rapidly decreasing flow demands, the system effectively becomes open loop and flow decreases no faster than  $1/t^2$ . Finally, Fig. 19 shows the system response to a unipolar sawtooth demand signal. Though the plots are somewhat busy, they reveal that the pressure feedback signal tracks well with the demand signal until the  $1/t$  response limit begins to dominate. Further, the plots indicate that the loop gain is sufficient to overcome the valve dead band at initiation of the demand pulse.

TIME	VDM1						VFWR	FLOW
.0	.0	X					.0	.0
2.0000E-02	.0	X					.0	.0
4.0000E-02	.0	X					.0	.0
6.0000E-02	10.000	I					X** 9.7730	5.8165
8.0000E-02	10.000	I					X** 9.7730	5.8165
.10000	10.000	I					X** 9.7730	5.8165
.12000	10.000	I					X** 9.7730	5.8165
.14000	10.000	I					X** 9.7730	5.8165
.16000	10.000	I					X** 9.7730	5.8165
.18000	10.000	I					X** 9.7730	5.8165
.20000	10.000	I					X** 9.7730	5.8165
.22000	.0	+		X	*		I 4.9831	1.5122
.24000	.0	+	X		*		I 3.3441	.68104
.26000	.0	+	X		*		I 2.5164	.38563
.28000	.0	+	X		*		I 2.0171	.24779
.30000	.0	+	X		*		I 1.6832	.17254
.32000	.0	+	X		*		I 1.4441	.12700
.34000	.0	+	X		*		I 1.2645	9.7376E-02
.36000	.0	X	*				I 1.1246	7.7025E-02
.38000	.0	X	*				I 1.0126	6.2446E-02
.40000	.0	X	*				I .92089	5.1646E-02
.42000	.0	X	*				I .84441	4.3423E-02
.44000	.0	X	*				I .77966	3.7018E-02
.46000	.0	X	*				I .72412	3.1933E-02
.48000	.0	X	*				I .67598	2.7828E-02
.50000	.0	X	*				I .63384	2.4466E-02
.52000	.0	X	*				I .59664	2.1679E-02
.54000	.0	X	*				I .56357	1.9342E-02
.56000	.0	X	*				I .53397	1.7364E-02
.58000	.0	X	*				I .50732	1.5674E-02
.60000	.0	X	*				I .48321	1.4220E-02
.62000	.0	X	*				I .46129	1.2959E-02
.64000	.0	X	*				I .44127	1.1858E-02
.66000	.0	X	*				I .42291	1.0892E-02
.68000	.0	X	*				I .40602	1.0039E-02
.70000	.0	X	*				I .39043	9.2832E-03
.72000	.0	X	*				I .37599	8.6093E-03
.74000	.0	X	*				I .36258	8.0062E-03
.76000	.0	X	*				I .35010	7.4643E-03
.78000	.0	X	*				I .33844	6.9756E-03
.80000	.0	X	*				I .32754	6.5334E-03
.82000	.0	X	*				I .31732	6.1319E-03
.84000	.0	X	*				I .30771	5.7664E-03
.86000	.0	X	*				I .29867	5.4325E-03
.88000	.0	X	*				I .29015	5.1269E-03
.90000	.0	X	*				I .28210	4.8463E-03
.92000	.0	X	*				I .27448	4.5882E-03
.94000	.0	X	*				I .26727	4.3501E-03
.96000	.0	X	*				I .26042	4.1301E-03
.98000	.0	X	*				I .25392	3.9264E-03
1.0000	.0	X	*				I .24773	3.7374E-03

(A) Plot of flow in torr-liters/second, pressure feedback signal and demand signal in volts.

Fig. 18. CSMP III simulation of closed-loop system response to a 150-ms demand pulse.

TIME	VDMI						VERR	VEA	VLVDRV
.0	.0	+-----0-----I-----X-I-----I					.10000	-1.0000	-15.000
2.0000E-02	.0	+ 0 I X I I					.10000	-1.0000	-15.000
4.0000E-02	.0	+ 0 I X I I					.10000	-1.0000	-15.000
6.0000E-02	10.000	I *I I I X 0 +					-.12705	1.2705	25.664
8.0000E-02	10.000	I *I I I X 0 +					-.12705	1.2705	25.664
.10000	10.000	I *I I I X 0 +					-.12705	1.2705	25.664
.12000	10.000	I *I I I X 0 +					-.12705	1.2705	25.664
.14000	10.000	I *I I I X 0 +					-.12705	1.2705	25.664
.16000	10.000	I *I I I X 0 +					-.12705	1.2705	25.664
.18000	10.000	I *I I I X 0 +					-.12705	1.2705	25.664
.20000	10.000	I *I-----I-----I-X-----0-->					-.12705	1.2705	25.664
.22000	.0	+ X 0 I I *					5.0831	-16.000	-15.000
.24000	.0	+ X 0 I *					3.4441	-16.000	-15.000
.26000	.0	+ X 0 I *					2.6164	-16.000	-15.000
.28000	.0	+ X 0 I*					2.1171	-16.000	-15.000
.30000	.0	+ X 0 * I I					1.7832	-16.000	-15.000
.32000	.0	+ X 0 * I I					1.5441	-15.441	-15.000
.34000	.0	+ X 0 * I I					1.3645	-13.645	-15.000
.36000	.0	+ X 0 * I I					1.2246	-12.246	-15.000
.38000	.0	+ 0 X * I I					1.1126	-11.126	-15.000
.40000	.0	+-----0-X-----I-----I-----I					1.0209	-10.209	-15.000
.42000	.0	+ 0 X* I I					.94441	-9.4441	-15.000
.44000	.0	+ 0 * X I I					.87966	-8.7966	-15.000
.46000	.0	+ 0 * X I I					.82412	-8.2412	-15.000
.48000	.0	+ 0 * X I I					.77598	-7.7598	-15.000
.50000	.0	+ 0 * X I I					.73384	-7.3384	-15.000
.52000	.0	+ 0 * X I I					.69664	-6.9664	-15.000
.54000	.0	+ 0 * X I I					.66357	-6.6357	-15.000
.56000	.0	+ 0 * X I I					.63397	-6.3397	-15.000
.58000	.0	+ 0 * X I I					.60732	-6.0732	-15.000
.60000	.0	+-----0-----X-----I-----I-----I					.58321	-5.8321	-15.000
.62000	.0	+ 0 * IX I I					.56129	-5.6129	-15.000
.64000	.0	+ 0 * IX I I					.54127	-5.4127	-15.000
.66000	.0	+ 0 * I X I I					.52291	-5.2291	-15.000
.68000	.0	+ 0 * I X I I					.50602	-5.0602	-15.000
.70000	.0	+ 0 * I X I I					.49043	-4.9043	-15.000
.72000	.0	+ 0 * I X I I					.47599	-4.7599	-15.000
.74000	.0	+ 0 * I X I I					.46258	-4.6258	-15.000
.76000	.0	+ 0 * I X I I					.45010	-4.5010	-15.000
.78000	.0	+ 0 * I X I I					.43844	-4.3844	-15.000
.80000	.0	+-----0-----I-X-----I-----I-----I					.42754	-4.2754	-15.000
.82000	.0	+ 0 * I X I I					.41732	-4.1732	-15.000
.84000	.0	+ 0 * I X I I					.40771	-4.0771	-15.000
.86000	.0	+ 0 * I X I I					.39867	-3.9867	-15.000
.88000	.0	+ 0 * I X I I					.39015	-3.9015	-15.000
.90000	.0	+ 0 * I X I I					.38210	-3.8210	-15.000
.92000	.0	+ 0 * I X I I					.37448	-3.7448	-15.000
.94000	.0	+ 0 * I X I I					.36727	-3.6727	-15.000
.96000	.0	+ 0 * I X I I					.36042	-3.6042	-15.000
.98000	.0	+ 0 * I X I I					.35392	-3.5392	-15.000
1.0000	.0	+-----0-----I-X-----I-----I-----I					.34773	-3.4773	-15.000

(B) Plot of valve drive, error amplifier output and input, and demand signals in volts.

Fig. 18 (continued)

TIME	PDDT						FLOW	VDM1
.0	.0	X					.0	.0
2.0000E-02	.0	X	I	I	I		+ .0	.0
4.0000E-02	.0	X	I	I	I		+ .0	.0
6.0000E-02	-.48749	I	I	I	I		* X 5.8165	10.000
8.0000E-02	-.48749	I	I	I	I		* X 5.8165	10.000
.10000	-.48749	I	I	I	I		* X 5.8165	10.000
.12000	-.48749	I	I	I	I		* X 5.8165	10.000
.14000	-.48749	I	I	I	I		* X 5.8165	10.000
.16000	-.48749	I	I	I	I		* X 5.8165	10.000
.18000	-.48749	I	I	I	I		* X 5.8165	10.000
.20000	-.48749	I					* X 5.8165	10.000
.22000	-3752.4	X +	*	I	I		I 1.5122	.0
.24000	-1689.9	X *	I	I +	I		I .68104	.0
.26000	-956.91	X *	I	I	I+		I .38563	.0
.28000	-614.87	X *	I	I	I		I .24779	.0
.30000	-428.13	X *	I	I	I		I .17254	.0
.32000	-315.15	X*	I	I	I		+ I .12700	.0
.34000	-241.63	X*	I	I	I		+ I 9.7376E-02	.0
.36000	-191.13	X	I	I	I		+ I 7.7025E-02	.0
.38000	-154.95	X	I	I	I		+ I 6.2446E-02	.0
.40000	-128.15	X					+ I 5.1646E-02	.0
.42000	-107.75	X	I	I	I		+ I 4.3423E-02	.0
.44000	-91.857	X	I	I	I		+ I 3.7018E-02	.0
.46000	-79.238	X	I	I	I		+ I 3.1933E-02	.0
.48000	-69.052	X	I	I	I		+ I 2.7828E-02	.0
.50000	-60.710	X	I	I	I		+ I 2.4466E-02	.0
.52000	-53.794	X	I	I	I		+ I 2.1679E-02	.0
.54000	-47.995	X	I	I	I		+ 1.9342E-02	.0
.56000	-43.086	X	I	I	I		+ 1.7364E-02	.0
.58000	-38.893	X	I	I	I		+ 1.5674E-02	.0
.60000	-35.284	X					+ 1.4220E-02	.0
.62000	-32.155	X	I	I	I		+ 1.2959E-02	.0
.64000	-29.424	X	I	I	I		+ 1.1858E-02	.0
.66000	-27.027	X	I	I	I		+ 1.0892E-02	.0
.68000	-24.912	X	I	I	I		+ 1.0039E-02	.0
.70000	-23.035	X	I	I	I		+ 9.2832E-03	.0
.72000	-21.363	X	I	I	I		+ 8.6093E-03	.0
.74000	-19.866	X	I	I	I		+ 8.0062E-03	.0
.76000	-18.522	X	I	I	I		+ 7.4643E-03	.0
.78000	-17.309	X	I	I	I		+ 6.9756E-03	.0
.80000	-16.212	X					+ 6.5334E-03	.0
.82000	-15.216	X	I	I	I		+ 6.1319E-03	.0
.84000	-14.309	X	I	I	I		+ 5.7664E-03	.0
.86000	-13.480	X	I	I	I		+ 5.4325E-03	.0
.88000	-12.722	X	I	I	I		+ 5.1269E-03	.0
.90000	-12.026	X	I	I	I		+ 4.8463E-03	.0
.92000	-11.385	X	I	I	I		+ 4.5882E-03	.0
.94000	-10.794	X	I	I	I		+ 4.3501E-03	.0
.96000	-10.248	X	I	I	I		+ 4.1301E-03	.0
.98000	-9.7429	X	I	I	I		+ 3.9264E-03	.0
1.0000	-9.2739	X					+ 3.7374E-03	.0

(C) Plot of demand in volts, flow in torr-liters/second, and  $dP/dt$  in torrs/second squared.

Fig. 18 (continued)

TIME	VDMI						VFWR	FLOW
.0	.0	X					.0	.0
8.0000E-03	.0	X		+		I	.0	.0
1.6000E-02	.0	X		+		I	.0	.0
2.4000E-02	.0	X		+		I	.0	.0
3.2000E-02	.0	X		+		I	.0	.0
4.0000E-02	.0	X		+		I	.0	.0
4.8000E-02	.0	X		+		I	.0	.0
5.6000E-02	.30000	X *		I +		I	.19173	2.2387E-03
6.4000E-02	.70000	I X *		I +		I	.59134	2.1296E-02
7.2000E-02	1.1000	I X *		I +		I	.99067	5.9769E-02
8.0000E-02	1.5000	I X *		I +		I	1.3897	.11762
8.8000E-02	1.9000	I X *		I +		I	1.7884	.19479
9.6000E-02	2.3000	I X *		I +		I	2.1868	.29124
.10400	2.7000	I X *		I +		I	2.5849	.40691
.11200	3.1000	I X *		I +		I	2.9826	.54176
.12000	3.5000	I X *		I +		I	3.3799	.69370
.12800	3.9000	I X *		I +		I	3.7769	.86872
.13600	4.3000	I X *		I +		I	4.1734	1.0607
.14400	4.7000	I X *		I +		I	4.5695	1.2716
.15200	4.9000	I X *		I +		I	4.7872	1.3956
.16000	4.5000	I X *		I +		I	4.3910	1.1742
.16800	4.1000	I X *		I +		I	3.9944	.97165
.17600	3.7000	I X *		I +		I	3.5973	.78806
.18400	3.3000	I X *		I +		I	3.2002	.62368
.19200	2.9000	I X *		I +		I	2.8423	.49200
.20000	2.5000	I X *		I +		I	2.5564	.39800
.20800	2.1000	I X *		I +		I	2.3228	.32858
.21600	1.7000	I X *		I +		I	2.1283	.27586
.22400	1.3000	I X *		I +		I	1.9639	.23488
.23200	.90000	I X *		I +		I	1.8230	.20239
.24000	.50000	I X *		I +		I	1.7010	.17621
.24800	9.9999E-02	I X *		I +		I	1.5943	.15480
.25600	-2.9802E-06	I X *		I +		I	1.5002	.13706
.26400	-2.9802E-06	I X *		I +		I	1.4166	.12221
.27200	-2.9802E-06	I X *		I +		I	1.3418	.10965
.28000	-2.9802E-06	I X *		I +		I	1.2745	9.8927E-02
.28800	-2.9802E-06	I X *		I +		I	1.2137	8.9705E-02
.29600	-2.9802E-06	I X *		I +		I	1.1584	8.1715E-02
.30400	-2.9802E-06	I X *		I +		I	1.1079	7.4746E-02
.31200	-2.9802E-06	I X *		I +		I	1.0616	6.8633E-02
.32000	-2.9802E-06	I X *		I +		I	1.0190	6.3240E-02
.32800	-2.9802E-06	I X *		I +		I	.97975	5.8458E-02
.33600	-2.9802E-06	I X *		I +		I	.94339	5.4199E-02
.34400	-2.9802E-06	I X *		I +		I	.90963	5.0389E-02
.35200	-2.9802E-06	I X *		I +		I	.87820	4.6967E-02
.36000	-2.9802E-06	I X *		I +		I	.84887	4.3883E-02
.36800	-2.9802E-06	I X *		I +		I	.82143	4.1092E-02
.37600	-2.9802E-06	I X *		I +		I	.79572	3.8559E-02
.38400	-2.9802E-06	I X *		I +		I	.77156	3.6254E-02
.39200	-2.9802E-06	I X *		I +		I	.74883	3.4149E-02
.40000	-2.9802E-06	I X *		I +		I	.72740	3.2223E-02

(A) Plot of flow in torr-liters/second, pressure feedback signal and demand signal in volts.

Fig. 19. CSMP III simulation of closed-loop system response to a 200-ms unipolar sawtooth demand signal.



TIME	PDOT						FLOW	VDMI
.0	.0	*					.0	.0
8.0000E-03	.0	*	X		+	I	.0	.0
1.6000E-02	.0	*	X		+	I	.0	.0
2.4000E-02	.0	*	X		+	I	.0	.0
3.2000E-02	.0	*	X		+	I	.0	.0
4.0000E-02	.0	*	X		+	I	.0	.0
4.8000E-02	.0	*	X		+	I	.0	.0
5.6000E-02	1535.4	*	I	X		I	+I 2.2387E-03	.30000
6.4000E-02	1534.0	I*	I	X		I	+I 2.1296E-02	.70000
7.2000E-02	1533.3	I*	I		X	I	+I 5.9769E-02	1.1000
8.0000E-02	1531.3	I					+I .11762	1.5000
8.8000E-02	1530.6	I	*	I		XI	+I .19479	1.9000
9.6000E-02	1529.5	I		*	I	I X	+I .29124	2.3000
.10400	1528.1	I		*	I	I X	+I .40691	2.7000
.11200	1526.5	I		*	I	I X	+I .54176	3.1000
.12000	1530.6	I		*	I	I X	+I .69570	3.5000
.12800	1523.1	I		*	I	I X	+I .86872	3.9000
.13600	1522.3	I		*	I	I X	+I 1.06607	4.3000
.14400	1520.7	I		*	I	I X	+I 1.2716	4.7000
.15200	-1520.0	I+		*	I	I X*	+I 1.3956	4.9000
.16000	-1522.6	I+		*	I	I X	+I 1.1742	4.5000
.16800	-1524.8	I+		*	I	I X	+I .97165	4.1000
.17600	-1519.1	I+		*	I	I X	+I .78806	3.7000
.18400	-1547.6	I+		*	I	I X	+I .62368	3.3000
.19200	-1220.8	I		*	I	I X	+I .49200	2.9000
.20000	-987.60	I		*	I	I X	+I .39800	2.5000
.20800	-815.34	I		*	I	I X	+I .32858	2.1000
.21600	-684.51	I		*	I	I X	+I .27586	1.7000
.22400	-582.82	I		*	I	I X	+I .23488	1.3000
.23200	-502.21	I		*	I	I X	+I .20239	.90000
.24000	-437.24	I		*	I	I X	+I .17621	.50000
.24800	-384.11	I	*		X		+I .15480	9.9999E-02
.25600	-340.11	I	*		X		+I .13706	-2.9802E-06
.26400	-303.25	I	*		X		+I .12221	-2.9802E-06
.27200	-272.08	I	*		X		+I .10965	-2.9802E-06
.28000	-245.48	I	*		X		+I 9.8927E-02	-2.9802E-06
.28800	-222.59	I	*		X		+I 8.9705E-02	-2.9802E-06
.29600	-202.77	I	*		X		+I 8.1715E-02	-2.9802E-06
.30400	-185.47	I	*		X		+I 7.4746E-02	-2.9802E-06
.31200	-170.30	I	*		X		+I 6.8633E-02	-2.9802E-06
.32000	-156.92	I	*		X		+I 6.3240E-02	-2.9802E-06
.32800	-145.06	I	*		X		+I 5.8458E-02	-2.9802E-06
.33600	-134.49	I	*		X		+I 5.4199E-02	-2.9802E-06
.34400	-125.04	I	*		X		+I 5.0389E-02	-2.9802E-06
.35200	-116.54	I	*		X		+I 4.6967E-02	-2.9802E-06
.36000	-108.89	I	*		X		+I 4.3883E-02	-2.9802E-06
.36800	-101.97	I	*		X		+I 4.1092E-02	-2.9802E-06
.37600	-95.681	I	*		X		+I 3.8559E-02	-2.9802E-06
.38400	-89.960	I	*		X		+I 3.6254E-02	-2.9802E-06
.39200	-84.737	I	*		X		+I 3.4149E-02	-2.9802E-06
.40000	-79.957	I	*		X		+I 3.2223E-02	-2.9802E-06

(C) Plot of demand in volts, flow in torr-liters/second, and dP/dt in torrs/second squared.

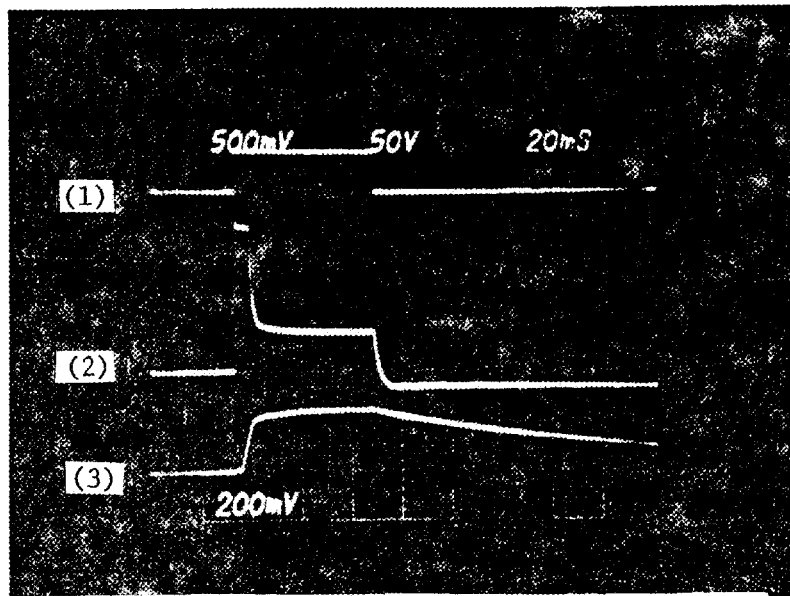
Fig. 19 (continued)

## 5. PRELIMINARY TEST RESULTS

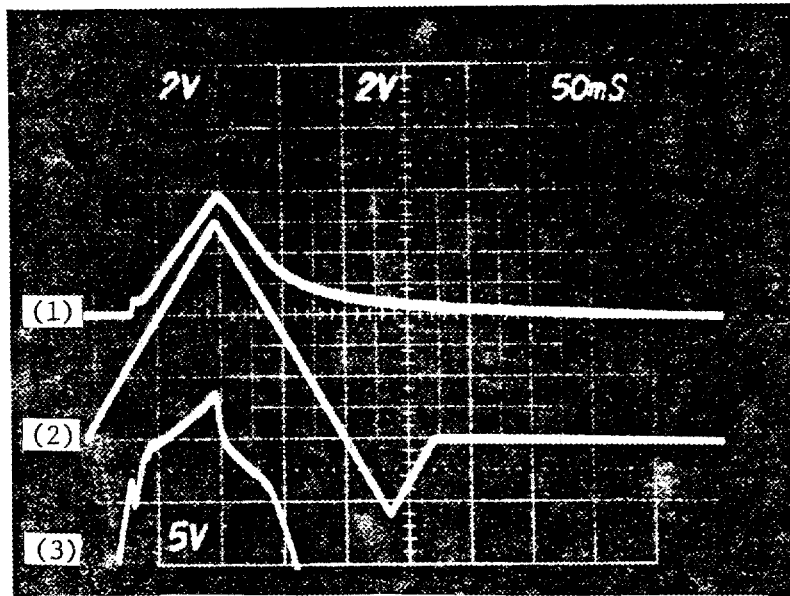
Qualitative results in laboratory tests with a slightly different gas injector were very similar to those seen in the computer simulation. Because of time constraints, calibrated and documented laboratory testing was not accomplished. The system was installed on the ISX Tokamak as soon as laboratory tests verified stability and proper operation. Oscilloscope photographs in Figs. 20 and 21 depict the qualitative system response to pulse, sawtooth, and sine demand functions. Figure 20(A) clearly depicts the operation of the valve popping circuit and the rapid pressure rise time as well as the relatively sluggish decay time. The remaining photographs [Figs. 20(B) and 21(A) and (B)] show the closed-loop response and the error amplifier output as the system attempts to track sawtooth and sine demand signals. The pressure glitch at the beginning of each trace is caused by pressure overshoot, which results from popping the gas valve open on a slowly varying demand signal.

After installation on the ISX, two fatal flaws surfaced. First, the thermal sensitivity of the pressure transducer resulted in an erroneous temperature signal of a magnitude approximately the same as the pressure signal. The character of the thermal signal was such that the composite signal appeared as a somewhat differentiated ( $dp/dt$ ) pressure signal, as indicated in Fig. 22(A). While the integral of the flow for a given input was repeatable, a meaningful calibration of flow to demand would have been a complex function and was not investigated.

The second flaw in the system surfaced when ISX's toroidal field was pulsed. Each time the field was activated, the induced signal drove the preamplifier output off-scale, as indicated in Fig. 22(B). The ISX experiment was terminated before the source of the noise coupling was confirmed, but preliminary results indicate that the noise was induced magnetically in the short cable connected between the transducer and the preamplifier. Detailed quantitative testing and calibration were, thus, never accomplished for this system. Development was suspended when the ISX experiment was terminated.

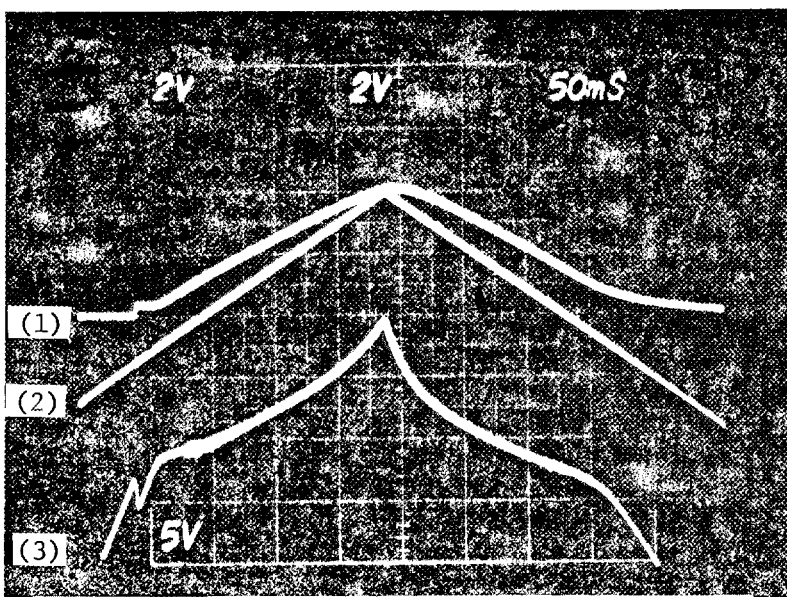


(A) Response to a 40-ms demand pulse. Trace 1 is the demand, trace 2 is the valve drive, and trace 3 is the pressure response.

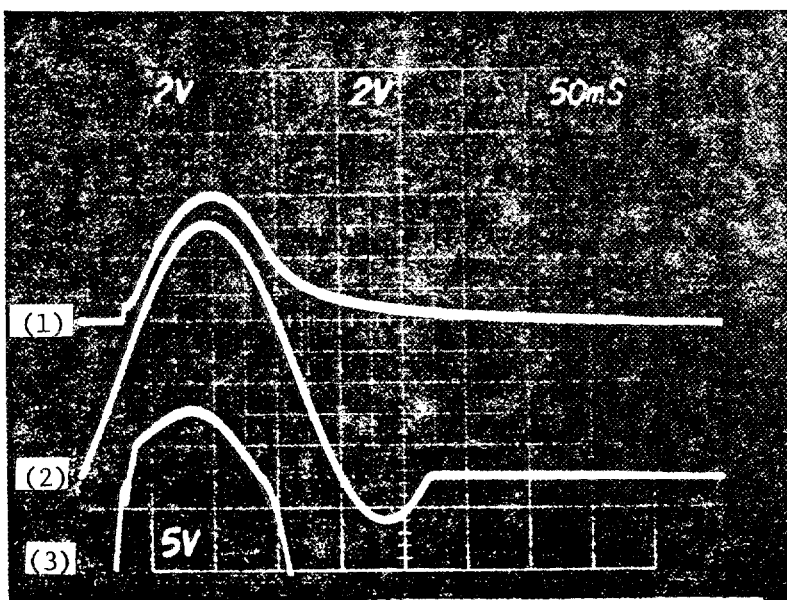


(B) Response to a 40-ms unipolar sawtooth demand pulse. Trace 1 is the pressure response, trace 2 is the demand, and trace 3 is the valve drive.

Fig. 20. Laboratory prototype response waveforms for short-duration demand signals.

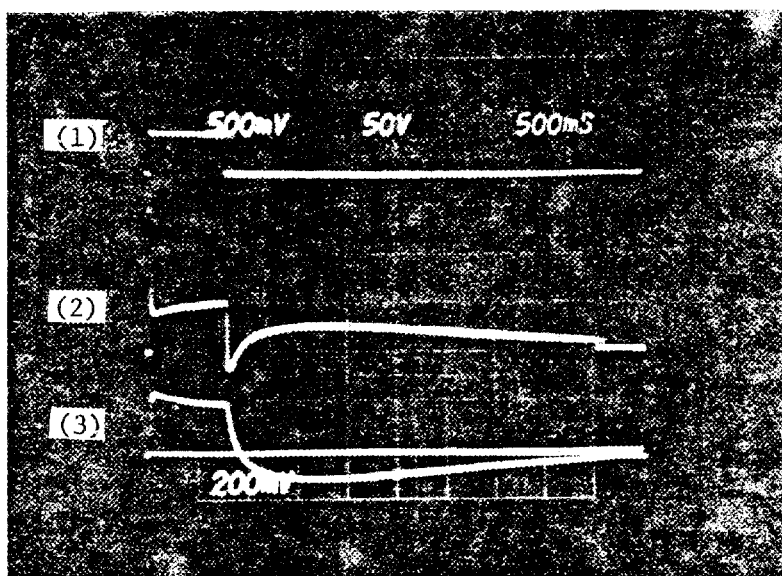


(A) Response to a 350-ms unipolar sawtooth demand. Trace 1 is the pressure response, trace 2 is the demand, and trace 3 is the valve drive.

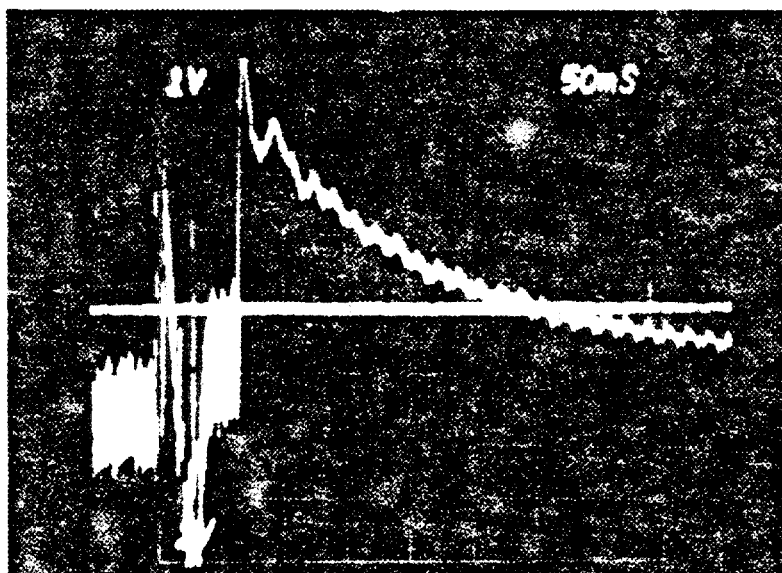


(B) Response to a 100-ms sinuous demand. Trace 1 is the pressure response, trace 2 is the demand, and trace 3 is the valve drive.

Fig. 21. Laboratory prototype response waveforms for long-duration demand signals.



(A) Thermal response. Trace 1 is the demand, trace 2 is the valve drive, and trace 3 is the pressure response. The tilt in the pressure response trace and the extension below the base line confirm an erroneous absolute pressure measurement.



(B) Noise intrusion of toroidal field power into the pressure signal with no demand signal. The straight trace is the pressure signal base line.

Fig. 22. Thermal and noise intrusion waveforms for the system installed on ISX-B.

## 6. CONCLUSIONS

The research efforts reported herein reinforce the feasibility of developing a fast gas-flow control system based on Poiseuille flow, provided a thermally inert fast pressure measurement technique can be perfected. Because of the extreme electromagnetic interference environment, however, this method does not appear to be a practical approach for Tokamak applications. For future attempts, it is suggested that consideration be given to summing an appropriate number of saturated flows (bits) to approximate the desired flow digitally in an open-loop injection system.

The injector tube from each valve could be sized for the desired flow with the valve fully open. Preinstallation calibration would then be possible, and one would need only to control the head pressure to ensure system accuracy and repeatability.

## REFERENCES

1. K. H. Burrell, "A Fast Hydrogen Gas Injection System for Plasma Physics Experiments," GA-A14604, General Atomic Company, September 1977. [Preprint of article in Rev. Sci. Instrum. 49, 948-54 (July 1978).]
2. K. H. Burrell, "Fast Hydrogen Gas Injection System for Plasma Physics Experiments;" Rev. Sci. Instrum. 49, 948-54 (July 1978).
3. S. Dushman and J. M. Lafferty, Scientific Foundations of Vacuum Techniques, 2nd ed., Wiley, New York, 1962, p. 82.
4. C. C. Gillispie, ed., Dictionary of Scientific Biography, Vol. XI, Scribner, New York, 1975, p.62.
5. J. F. Pierce and T. J. Paulus, Applied Electronics, Charles E. Merrill, Columbus, Ohio, 1972.
6. F. H. Speckhart and W. L. Green, A Guide to Using CSMP-The Continuous System Modeling Program, Prentice-Hall, Englewood Cliffs, N.J., 1976.

Additional Background Material

- S. C. Bates and K. H. Burrell, "Fast Gas Injection System for Plasma Physics Experiments," Rev. Sci. Instrum. 55, 934-39 (June 1984).



ORNL/TM-10660  
Dist Category UC-37  
Instruments

## INTERNAL DISTRIBUTION

- |                          |   |
|--------------------------|---|
| 1. H. R. Brashear        | 13. M. J. Kopp (Advisor)                                  |
| 2. B. G. Eads            | 14. P. F. McCrea (Advisor)                                |
| 3. D. N. Fry             | 15. H. M. Paynter (Advisor)                               |
| 4. W. R. Hamel           | 16-17. Central Research Library                           |
| 5. D. R. Miller          | 18. Y-12 Document Reference<br>Library                    |
| 6. J. A. Moore           | 19-20. Laboratory Records                                 |
| 7. C. A. Mossman         | 21. Laboratory Records - RC                               |
| 8. C. H. Nowlin          | 22. ORNL Patent Section                                   |
| 9. R. A. Todd            | 23. I&C Publications and<br>Information Processing Center |
| 10. D. Webber            |   |
| 11. R. S. Wiltshire      |   |
| 12. J. B. Ball (Advisor) |   |

## EXTERNAL DISTRIBUTION

24. Assistant Manager for Energy Research and Development, U.S.  
Department of Energy, Oak Ridge Operations, Oak Ridge, TN 37831
- 25-129. Given distribution under Category UC-37, instruments

